Evidence of a dual African and Australian biomass burning influence on the vertical distribution of aerosol and carbon monoxide over the Southwest Indian Ocean basin in early 2020

Nelson Bègue[1], Alexandre Baron[2,3], Gisèle Krysztofiak[4], Gwenaël Berthet[4], Hassan Bencherif[1,5], Corinna Kloss[4]*, Fabrice Jégou[4], Sergey Khaykin[6], Marion Ranaivombola[1], Tristan Millet[1], Thierry Portafaix[1], Valentin Duflot[1,], Philippe Keckhut[6], Hélène Vérèmes[1], Guillaume Payen[7], Mahesh Kumar Sha[8], Pierre-François Coheur[9], Cathy Clerbaux[9,10], Michaël Sicard[1], Tetsu Sakai[11], Richard Querel[12], Ben Liley[12], Dan Smale[12], Isamu Morino[13], Osamu Ochino[11,13], Tomohiro Nagai[11], Penny Smale[12] and John Robinson[12]**

[1] Laboratoire de l'Atmosphère et des Cyclones, UMR 8105 CNRS, Université de la Réunion, Reunion Island, France.

[2] Cooperative Institute for Research in Environmental Sciences (CIRES), University of Colorado, Boulder, CO 80305, USA

[3] NOAA Chemical Sciences Laboratory (CSL), 325 Broadway, Boulder, CO 80305, USA

[4] Laboratoire de Physique et Chimie de l'Environnement et de l'Espace (LPC2E), Université d'Orléans, CNRS UMR7328, Orléans, France.

[5] School of Chemistry and Physics, University of KwaZulu-Natal, Durban 4041, South Africa

[6] Laboratoire Atmosphères, Observations Spatiales (LATMOS), IPSL, UVSQ Université Paris-Saclay, Sorbonne Université, CNRS, Guyancourt, France

[7] Observatoire des Sciences de l'Univers de La Réunion (OSU-Réunion), UAR3365, Saint-Denis de la Réunion, France

[8] Royal Belgian Institute for Space Aeronomy (BIRA-IASB), Brussels, Belgium

[9] Université libre de Bruxelles (ULB), Spectroscopy, Quantum Chemistry and Atmospheric Remote Sensing (SQUARES), Brussels 1050, Belgium; Bruxelles (ULB), Brussels 1050, Belgium.

[10] Laboratoire Atmosphères, Observations Spatiales (LATMOS), IPSL, Sorbonne Université, UVSQ, CNRS, Paris, France

[11] Meteorological Research Institute, 1-1 Nagamine, Tsukuba, Ibaraki 305-0052, Japan

[12] National Institute of Water & Atmospheric Research (NIWA), Lauder, New Zealand

[13] National Institute for Environmental Studies, Tsukuba, Japan

***now at : Institute for Energy and Climate Research - Stratosphere (IEK-7), Forschungszentrum Jülich, Jülich, Germany**

****now at : Department for Atmospheric and Climate Research, NILU – Norwegian Institute for Air Research, Kjeller, Norway**

Correspondence to: N.Bègue (nelson.begue@univ-reunion.fr)

Abstract

The pristine atmosphere of the southwest Indian Ocean (SWIO) basin underwent significant perturbations during the 2020 austral summer. This study documents the complex variability of aerosols and carbon monoxide (CO) over this remote oceanic region and identifies the processes governing it in the upper troposphere – lower stratosphere (UT-LS). Aerosol profiles exhibit a multi-layer structure in the tropical UT-LS in January and February 2020. The numerical models (FLEXPART and MIMOSA) showed that the modulation of the aerosol content in the lower stratosphere is due to the intense and persistent stratospheric **aerosol layer** generated during the 2019-20 extreme Australian bushfire events. One part of this stratospheric **aerosol layer** was advected zonally by the prevailing easterly winds and its passage over Reunion was recorded by increased aerosol extinction profiles on 27th and 28th January. The analysis of the advected potential vorticity highlights an isentropic transport of air masses containing Australian biomass burning aerosol from extra-tropical latitudes to Reunion at the 400 K isentropic level, on 28th January. Interestingly, our results show that the **biomass burning (BB)** activity in eastern Africa, weak during this season, contributed to **modulating** (**by** up to 90%) the vertical distribution of CO and aerosols in the upper troposphere over the SWIO basin. The simultaneous presence of African and Australian **aerosol layers** has been recorded by ground-based observations at Reunion. This study highlights for the first time the influence of the African emissions from BB to the CO and **aerosol** distribution in the upper troposphere over the SWIO basin during the convective season. The results show that besides PyroCb -driven injection of BB products to the stratosphere, an alternative pathway may exist during the regular deep-convection season in the tropics.

1. Introduction

Large amounts of aerosols and active trace gases such as carbon monoxide (CO) are injected throughout the atmosphere during biomass burning (BB) events. The Southern American and Southern African regions are recognized to be significant primary sources of carbonaceous aerosol and active traces gases in the Southern Hemisphere through the BB season from July to November (Bencherif et al., 2020; Garstang et al., 1996; Holanda et al., 2020). Such BB

activities have the potential to modulate the vertical distribution of trace gases and aerosols from the troposphere to the stratosphere (Andreae and Merlet, 2001; Duflot et al., 2010; Héron et al., 2020). Under favorable meteorological conditions, pyro-convection events can take place and have the potential to inject soot and smoke directly into the stratosphere (Dowdy and Pepler, 2018; Fromm et al., 2010). Radiative impact of the **aerosol** and traces gases is determined by abundance, vertical distribution, and atmospheric residence time (which, in turn, will affect the resultant horizontal distribution following advection (Darbyshire et al., 2018; Morgan et al., 2019)). High concentrations of trace gases and **aerosol** from these fires can be transported far from the source regions. This intercontinental transport has the potential to affect the atmospheric composition of regions **typically** considered as aerosol-free areas.

The southwest Indian Ocean (SWIO) basin is known to be one of the few pristine regions on Earth where the aerosol concentration is mainly governed by sea salts (Duflot et al., 2022). The SWIO basin is characterized by a wet season (December to April) and a dry season (May to November). Previous works showed that the atmospheric composition over the SWIO region during the dry season is driven by the Southern Hemisphere BB activity (Clain et al., 2009; Duflot et al., 2022; Edwards et al., 2006; Kaufman et al., 2003, Swap et al., 2003). These studies pointed out that BB plumes cross South Africa during the dry season. Edwards et al. (2006) revealed that southern African BB emissions mostly find their way into the SWIO basin and follow the five transportation modes identified by Garstang et al. (1996). Being located in the subtropical southern Indian Ocean at the crossroads of the transport pathway bringing air masses from southern Africa, Reunion Island (21,0°S, 55.5°E) is a favorable location to study the effect of this regional transport on atmospheric composition over the SWIO basin. Based on ozone radiosonde and ground-based lidar observations recorded at Reunion, Clain et al. (2009) highlighted a significant annual increase of tropospheric ozone over Reunion Island during August-November period, in phase with the BB season in southern Africa and Madagascar. High concentrations of ozone precursors from these fires are vented into the free troposphere by convection and are subsequently advected into the SWIO basin by westerly winds. In addition to regional transport, the tropical tropospheric composition over the SWIO basin can be modulated by the long-range transport of BB plumes from South America (Duflot et al., 2010, 2022; Zhou et al., 2018). By combining ground-based observations of Carbon monoxide (CO) from a Fourier Transform Infrared (FTIR) spectrometer installed at Reunion and the FLEXPART model simulations, Duflot et al. (2010) showed that southern African and southern American BB events have the potential to inject large amounts of ozone precursors such as CO and aerosols throughout the troposphere over the SWIO basin. The synergy of CO

and **aerosol** observations are helpful in discussions of the influence of BB events on the evolution of the aerosol burden (Bègue et al., 2021; Bencherif et al., 2020; Jones et al., 2001). Most recently, the analysis of **Aerosol** Optical Depth (AOD) recorded from sun-photometer at Reunion over a period of 12-years has been undertaken by Duflot et al. (2022). They showed that the BB activity explains 67 % of the variability of the AOD, within which the contributions of the BB activity in Southern Africa and southern America are estimated at 22% and 20%, respectively. Although Australia is known for its intense BB events (Fromm et al., 2006; 2010; De Laat et al., 2012), the contribution of the Australian BB activity on the observed AOD variability over Reunion is relatively low (4.7 %).

The Australian BB activity takes mainly place in the northern part of the continent between September and January (Russel-Smith et al., 2007). Nevertheless, the most disastrous fires burn in the southeastern region of Australia. Extreme fires occurring over southeastern Australia during the austral summer can lead to the development of pyro-convection events (Dowdy and Pepler, 2018; Fromm et al., 2010). Southeastern Australia has a long history of severe pyro-convection events which have significantly impacted the composition of the stratosphere at regional and global scales. The last and largest event occurred during the 2019-20 fire season (referred to as "Black Summer"). Previous works reported that this fire season is unrivaled with a surface burnt estimated at 19 million hectares (Boer et al., 2020; Cai et al., 2022; Levin et al., 2021). Furthermore, this extreme fire season can be considered as unprecedented due to persistent planetary-scale perturbations induced in the stratosphere (Kablick et al., 2020; Khaykin et al., 2020; Kloss et al., 2021; Ohneiser et al., 2020, 2022; **Santee et al., 2022; Schwartz et al., 2020; Solomon et al., 2023;** Yu et al., 2020).

Kablick et al. (2020) showed at least 18 pyro-convection outbreaks occurred between 29th December 2019 and 12th January 2020 with the largest event occurring around 1st January 2020. Based on satellite observations and **Community Earth System Model- Community Aerosol and Radiation Model for Atmospheres (CESM-CARMA)** model results, Yu et al. (2021) showed that Australian wildfires burning from December 2019 to January 2020 injected approximately 0.9 Tg of smoke into the stratosphere. The analysis of the numerical simulations suggest that the smoke mass contained 2.5% black carbon which induced a 1 K warming in the stratosphere of the Southern Hemisphere mid-latitude for more than 6 months following its injection. The carbon-rich aerosol clouds were confined during their solar-driven rise by a persistent synoptic-scale anticyclone (Kablick et al., 2020; Khaykin et al., 2020). As a consequence, the highly-concentrated absorbing aerosols were lofted into the middle stratosphere, which prolongs their stratospheric residence time and radiative effect on climate.

The combustion products injected into the stratosphere were advected by westerly winds and dispersed across all of the Southern Hemisphere extra-tropical latitudes (Khaykin et al., 2020; Ohneiser et al., 2020, 2022; Tencé et al., 2022; Yu et al., 2020). The stratospheric smoke layer was rapidly advected westward and its optical characteristics were measured by the lidar system installed at Punta Arena (53.2°S, 70.9°E; Chile) and Rio Grandé (53.8° S, 67.7° W, Argentina) one week following its injection (Ohneiser et al., 2022). Ohneiser et al. (2022) pointed out that the presence of the smoke layers extended, on average, from 9 to 24 km in height, with one part ascending to more than 30 km height as a result of self-lofting processes. The maximum smoke AOD was around 1.0 over Punta Arenas in January 2020 and thus 2 to 3 orders of magnitude above the stratospheric aerosol background of 0.005 (Ohneiser et al., 2022). Their results suggest an influence of this stratospheric smoke layer on the record-breaking ozone hole over Antarctica in September-November 2020. This is consistent with the results reported by Tencé et al. (2022) from lidar and ozonesondes measurements at the French Antarctic station Dumont d'Urville (66.6°S,140.0°E). Tencé et al. (2022) pointed out the persistence of **an aerosol layer** in the southern high-latitude stratosphere following the pyro-convection events. They also reported that the 2020 stratospheric ozone depletion is above the decadal average at Dumont d'Urville. The common point among these studies is their interest for the perturbation induced by the 2019-20 Australian fires on the stratospheric composition, and on the dynamical circulation over the extra-tropical latitudes. In contrast, relatively little attention has been paid to the perturbation induced by **this Australian BB layer** over the tropical/subtropical latitudes. This study has two aims: 1) document the transport of the Australian smoke layer in the southern subtropics over Indian Ocean during the January-February period which correspond to the wet season, and 2) to investigate the influence of Australian **aerosol layer** on variability of the aerosol optical properties and CO in the Upper Troposphere-Lower Stratosphere (UT-LS) of the SWIO basin accounting for convective activity. Convective activity is more intense during this season as the Inter-Tropical Convergence Zone (ITCZ) is present over the whole basin (Lashkari et al., 2017). Furthermore, the convective activity is often synonym of tropical depression which can reach the stage of tropical cyclone (Barthe et al., 2021; Neuman et al., 1993). The Regional Specialized Meteorological Centre (RSMC) at Reunion reported that the cyclonic season 2019-20 was characterized by the development of 6 tropical cyclones and 4 tropical storms in the SWIO basin.

The study is organized as follows: Section 2 describes the observations and the model used for the investigation of the transport of the **aerosol layer**. A review of the formation and the transport of the Australian **aerosol layer** over the Southern Hemisphere is provided in Section

3. An analysis of the influence of **the Australian BB plume** on the aerosol and CO variability over the SWIO basin is given in Section 4. The discussion on the influence of the convective activity on the transport of the aerosol smoke layer over the SWIO basin is provided in Section 5. A summary and the perspectives of this study are given in Section 6.

2. Instrumentation and Model description

2.1 Aerosols data sets

The aerosol datasets used in this study resulted mainly from two ground-based observations sites from the Network for the Detection of Atmospheric Composition Change (NDACC, www.ndacc.org) network as well as a suite of spaceborne sensors products.

2.1.1 Lauder ground-based lidar

Aerosol optical properties measurements at Lauder (45.0°S; 169.7°E) have been performed using lidars since 1992. A detailed description of the lidar system operating at Lauder is given by Sakai et al. (2016), and it is summarized hereafter. The emitter system consists of a Nd:YAG laser beam at 532 nm and is linearly polarized. The lidar detects Rayleigh-Mie backscattering at 532 nm with parallel and perpendicular components. The methodology described by Fernald et al. (1984) is used to obtain the extinction and backscatter coefficient from a Rayleigh-Mie lidar. This methodology involves the use of an extinction-to-backscatter ratio for aerosol, also called lidar ratio (LR). For the January-May 2020 period, the values of LR derived with the lidar, are 88 and 60 sr for altitude above and below 23 km respectively. These values are obtained from the attenuation of the lidar signals by using the methodology described by Uchino et al. (1983) and by Young (1995). The aerosol depolarization is computed from the backscatter coefficient and the total linear volume depolarization ratio (Sakai et al., 2003). This latter is obtained by taking the ratio of the perpendicular to total components of the backscattered signal at 532 nm. To investigate the aerosol variability induced by the Australian fires, it is **necessary** to define a background profile. **Such a profile** is built from measurements performed when atmosphere is not undergoing major disturbance (e.g, volcanic eruptions, pyro-convection outbreaks). In the present work, the background extinction profile at Lauder is built from measurements performed between 1997 and 2004.

2.1.2 Reunion Island ground-based lidars

The Atmospheric Physics Observatory of La Réunion (OPAR) is a permanent station for long term atmospheric observations (Baray et al., 2013). In particular, two lidar systems operating in the UV (355 nm) and visible part of the light spectrum (532 nm) are used to retrieve ozone and aerosols profiles at the Maïdo Observatory situated at 2200 m above mean sea level

(AMSL). These systems, named LiO3T (532 nm) and LiO3S (355 nm) are described by Baray et al. (2006). These lidars measure aerosol optical properties (extinction, backscatter ratio) from ~15 km to the middle stratosphere, up to ~35 km, with a high vertical resolution (15 m). Operating at two distinct wavelengths, the synergy of Reunion lidar profiles allows us to assess the Angström exponent of aerosols between 355 nm and 532 nm. **The Angström exponent is a parameter informing on the extinction behavior of the atmospheric constituent with the light spectrum. It is often used to infer some microphysical properties of aerosol and in particular some information on the particle size. In general, a small Angström exponent is synonym of a coarse mode driving the optical properties of the aerosol. Insight on the Angström exponent and aerosol size as well as its relative error with respect to extinction properties are developed in Baron, et al, 2023 and its attached supplementary information.** In this study, the inversion process used the Klett method (Klett, 1985) with an assumed lidar ratio of 60 sr, typical of aged BB aerosols (Müller et al., 2007). In the present study we used 9 lidar profiles recorded during the January-March 2020 period. The background extinction profile at Reunion is built from measurements performed between 2017 and 2019 excluding the perturbation induced by the Calbuco eruption in April 2015 (Bègue et al., 2017). **Although the lidar systems used in this study are different builds, extinction profiles at 532 nm from Lauder and Reunion can be compared to infer the evolution of the plume optical properties.**

2.1.3 CALIOP

Cloud-Aerosol Lidar with Orthogonal Polarization (CALIOP) is a nadir pointing lidar orbiting the Earth onboard the Cloud-Aerosol Lidar and Infrared Pathfinder Satellite Observation (CALIPSO) satellite since 2006. CALIOP is a two-wavelength polarization-sensitive lidar (532 and 1064 nm) that measures total attenuated backscatter vertical profiles with altitude-varying vertical (30–300 m) and horizontal (300–5000 m) resolution. In the present study, we used CALIOP product version 3.3 level 1B which includes calibrated attenuated backscatter along with collocated meteorological information provided by the National Aeronautics and Space Administration Global Modeling and Assimilation Office (GMAO). These data are postprocessed using a treatment described and validated by Vernier et al. (2009). The Scattering Ratio (SR) profiles used for the detection of the smoke plume are calculated following the methodology described by Khaykin et al. (2018). As a first step, the collocated GMAO data is used to correct the backscatter profiles of molecular attenuation and ozone absorption. Then, the SR is calculated as the ratio of total and molecular backscatter coefficients, with the latter derived from GMAO air density. The SR profiles are recalibrated at 36-39 km, following the

methodology given by Vernier et al. (2009). The data with depolarization larger than 30 % are discarded to the treatment in order to avoid aliasing cirrus clouds above the thermal tropopause. The CALIOP data were obtained from the ACDISC data archive (ftp://acdisc.gsfc.nasa.gov) hosted by NASA Goddard Space Flight Center.

2.1.4 Sun photometry measurements: Sky radiometer

A sky radiometer is a scanning sun-sky photometer able to perform measurements of direct sun and diffuse sky irradiance under clear sky conditions, at seven wavelengths (between 315 and 1020 nm) and at several scattering angles. The direct solar extinction and diffuse sky radiance measurements are used to derive the aerosol optical properties such as Aerosol Optical Depth (AOD), Single Scattering Albedo (SSA) and aerosol size-distributions using the algorithm developed by Nakajima et al. (1996). A detailed description of the sky radiometer and the associated data retrieval is given by Hashimoto et al. (2012). In the present study, we used the sky radiometer observations performed at Lauder in the framework of the SKYNET network. SKYNET is a ground-based network of sky radiometers with observation sites spread over Asia and other areas. Previous works have shown that the AOD from SKYNET is obtained with high accuracy similar with that of the standard Langley method and with those from AERONET (Campanelli et al., 2007; Che et al., 2008). At Lauder, the sky radiometer measurements have been made since 2011. These observations are used in the present study to investigate the aerosol variability induced by the passage of the Australian BB plume over Lauder. The background evolution of AOD is built with measurements performed between 2011 and 2018. The sky radiometer data used in this work are available on: https://www.skynet-isdc.org/

2.1.5 OMPS-LP

The Ozone Mapper and Profiler Suite Limb profiler (OMPS-LP) has been flying on the Suomi National Polar Partnership (NPP) satellite platform since October 2011. In the present study, we use aerosol extinction profile from the NASA OMPS data product version 2.0 (Taha et al., 2021). The aerosol extinction profiles are retrieved from the limb scattering solar radiation. The V2.0 algorithm uses OMPS-LP measurements at wavelengths 510, 600, 675, 745, 869 and 997 nm, selected to minimize the effect of gaseous absorption (Taha et al., 2021). Aerosol extinction measurements are provided from 10 to 40 km altitude on a 1 km vertical grid. A near-global coverage is produced within 3-4 days. The OMPS data are used in the present study to investigate the global transport of aerosol BB plume and its influence on the aerosol variability over Reunion. As recommended by Taha et al. (2021), we use aerosol extinction measurements at 745 nm. The background extinction profile is built with measurements performed from 2012 to 2014 and from 2016 to 2018. These periods are chosen in order to discard the perturbation

induced by the Calbuco eruption (Bègue et al., 2015). The OMPS data are downloaded from: https://ozoneaq.gsfc.nasa.gov/.

The aerosol absorbing index (AAI) data from OMPS are also used to describe the transport of the aerosol BB plume. This index allows the detection of absorbing aerosols through the spectral difference between a given pair of UV wavelength. When its value is positive, it indicates the presence of UV-absorbing aerosols such as dust and smoke. Conversely, a negative value indicates the presence of non-absorbing aerosols while values close to zero are found in the presence of clouds. The AAI data used in this work are available on the NASA Earth Data platform: https://earthdata.nasa.gov/earth-observation-data

2.2 CO and water vapor measurements

2.2.1 FTIR

The total columns and volume mixing ratio profiles of trace gases such as CO are retrieved with high accuracy and precision with ground-based Fourier Transform Infrared (FTIR) spectrometers (Clerbaux et al., 2008; Vigouroux et al., 2015; Zhou et al., 2019). In the present study, we use the FTIR observations performed at Lauder and Reunion sites in the framework of the NDACC and Total Carbon Column Observing Network (TCCON) networks respectively. A detailed description of the FTIR systems involved in both networks and the associated data retrieval is given by De Mazière et al. (2018) and Wunch et al. (2015). A brief description is given hereafter. The CO measurements from FTIR at Lauder have been made since the early 1990s. The measurements are made using a Bruker high-resolution spectrometer over a wide spectral range (around 600–4500 cm^{-1}). The CO dataset used in this study is the same as that used by Bègue et al., (2021) and Kloss et al., (2019). Details on the spectral measurements, CO retrieval strategy and derived CO column abundances can be found within these references. The CO total columns and volume mixing ratio profiles on 48-layer atmosphere (0.37–100 km asl) used in this study for the Lauder site **were** downloaded from the NDACC website (http://www.ndacc.org).

The FTIR measurements at Reunion have been routinely performed in the framework of the TCCON network since 2011. A Bruker high-resolution spectrometer over a wide spectral range is also used at Reunion. The CO and O_2 total columns are simultaneously retrieved by using the GGG2014 code (Wunch et al., 2015). Column-averaged dry-air mole fraction of CO are obtained from the retrieval of these two components. TCCON uses the O_2 total to determine the total column of the dry air. Then, the column-averaged dry-air mole fraction of CO is calculated as the ratio between the retrieved CO total columns and the total columns of the dry air. The abundance of CO used in the study for Reunion are downloaded from the TCCON

database (https://tccondata.org). In the present study, the background evolution of CO is built with measurements performed between 2015 and 2018 (De Mazière et al., 2017).

2.2.2 IASI

The Infrared Atmospheric Sounding Interferometer (IASI) measures chemical species such as CO by using a Fourier Transform spectrometer (Clerbaux et al., 2009; Coheur et al., 2009). It is flying onboard the three Metop satellites. Retrieval of CO total and partial columns occurs in near real-time from the nadir radiances measured by the instrument in the thermal infrared, covering wavelengths from 6.62 to 15.5 µm. Global distributions are obtained for day and night measurements, with a vertical range covering the troposphere and the lower stratosphere. The total and partial column of CO are retrieved by using the Fast-Optimal Retrievals on Layers for IASI (FORLI-CO, Hurtmans et al., 2012). Furthermore, the contamination of the data by clouds is checked and flagged. In the present study, we used CO columns from IASI instruments on Metop-A and Metop-B, which have been operating since 2006 and 2012, respectively. The IASI products used in this work are available on the AERIS platform: https://iasi.aeris-data.fr/CO.

2.2.3 MLS

The Microwave Limb Sounder (MLS) performs vertical profile measurements of multiple trace gases in the UT-LS onboard Aura satellite since 2004 (Waters et al., 2006). In the present study, the CO and water vapor observations (version 5) from January 2017 to January 2020 over a global domain extending between 10°S and 25°S in latitude and 30°E and 60°E in longitude have been used. All MLS version 5 retrieval quality flags (quality, status, convergence, and precision) were properly adhered to for all of our analyses (Livesey et al., 2020). Generally, recommended pressure levels for science applications with CO and water vapor MLS data range from 0.0215 to 215 hPa (Version 5.0x Level 2 and 3 data quality and description document. (nasa.gov)). The CO and water vapor profiles from MLS are obtained from the Atmospheric Composition Data and Information Services Center (ACDISC) archive (ftp://acdisc.gsfc.nasa.gov) hosted by the NASA Goddard Space Flight Center.

2.3 Numerical Modelling

2.3.1 FLEXPART Model

The Lagrangian transport and diffusion model FLEXPART version 10.4 is used to simulate long-range transport of atmospheric tracers (Pisso et al., 2019; Stohl et al., 2005). This version of FLEXPART includes improvements in different aspects such as **microphysical and chemical** parameterizations (Pisso et al., 2019). Source identification occurs via the release of particles from a receptor location and the simulation of backward trajectories. Model calculations are based on ERA5 (Hersbach et al., 2020) meteorological data from the European

Center for Medium-Range Weather Forecasts (ECMWF) extracted at 3-hourly intervals with a horizontal resolution of 0.5° × 0.5° and a vertical resolution of 137 hybrid model levels (from the ground to 0.01 hPa pressure altitude).

The model simulations are run with the aerosol **(Black Carbon-BC and Organic Carbon-OC)** and CO tracers assuming removal by dry and wet deposition for aerosols and OH reactions for CO **by using parameter from Pisso et al. (2019).** Each simulation consists of 20,000 particles released over Reunion during one day at altitudes between 15 and 19 km every 0.5 km and followed backward in time during one month. The simulation of backward trajectories with FLEXPART for a long period (1-2 months) were previously explored in previous studies (Aliaga et al., 2021; Eckhardt et al., 2017; Xu et al., 2021). The simulations include the parameterization of turbulence and the activation of the convection. FLEXPART model outputs are distributed over a regular vertical grid of 0.5°x 0.5° from ground to 25 km in altitude. The model outputs are used to discuss the residence time of the BB aerosols and CO, and their contributions on the variability of the aerosol optical properties and CO over the SWIO basin. Discussions are based on the analysis of the emission sensitivity obtained from backward simulations. The residence time of particles are integrated over the entire atmospheric column and over the latitude to create averaged-map and longitudinal cross-section map and to provide information on the geographical and vertical dispersion of BB aerosols in the atmosphere. The BB contributions on the vertical distribution of CO and the aerosol optical properties can be calculated by combining the potential emission sensitivity (PES) with an emission inventory. PES represents FLEXPART particles only in the layer/altitude at which the emissions are injected. Pyro-convection is not **taken** into account in the model (nor ECMWF data). **A** mass concentration profile of BB aerosol and CO is extracted by summing all the output grid-points. A layer between 0 and 3 km is used for the BB in Africa (as observed in the **Global Fire Assimilation System** "top altitude of plume", Kaiser et al., 2012) and between 9 and 16 km for the Australian fires (as observed by CALIOP).

In the present study, the **Global Fire Assimilation System (GFAS)** version 1.2 emission (Kaiser et al., 2012) has been used for the calculation. In addition, the Global Air Pollutant Emissions - EDGAR v6.1 emission inventory (Kaiser et al., 2012, http://edgar.jrc.ec.europa.eu) is used for CO for the year 2018 with a 0.1° × 0.1° grid. These emissions represent the total CO emissions by anthropogenic activities excluding large scale BB from Savannah burning and forest fires. As for the BB emissions, multiplying the CO emission flux from this inventory with the FLEXPART emission sensitivity for a layer between 0 and 1 km gives access to the contribution of anthropogenic sources to the total CO abundance. At the end of the process, in

the case of aerosols, the mass concentration profile is converted in extinction profile in order to **evaluate** the contribution of BB aerosols on the vertical distribution of the aerosol extinction observed from Lidar over Reunion. The conversion is performed by the use of Mie scattering model assuming spherical particles with a density of 2 g.cm^{-3} and a refractive index of 2.0 + 0.64i adapted to optically absorbing aerosols.

2.3.2 MIMOSA Model

The Modèle Isentropique de transport Mésoéchelle de l'Ozone Stratosphérique par Advection (MIMOSA) model is a potential vorticity (PV) advection model running on isentropic surfaces at a resolution of 0.3° × 0.3° (Hauchecorne et al., 2002). The advection scheme is semi-Lagrangian with a time step of 1 h and driven by **ERA5 reanalysis meteorological outputs**. The model can be run continuously in order to follow the evolution of PV filaments for several months. The accuracy of the model has been evaluated by Hauchecorne et al. (2002) and validated against airborne lidar ozone measurements using a correlation between PV and ozone, a quasi-conserved chemical tracer on timescales of a week or so within most of the lower stratosphere (Heese et al., 2001). The MIMOSA model can also be used to determine the origin of air masses influencing a given site, similar to an isentropic Lagrangian trajectory model (Bencherif et al., 2011; Hauchecorne et al., 2002; Portafaix et al., 2003; Bègue et al., 2017).

3. Formation of an intense stratospheric BB plume over Australia

Following the strongest outbreak during New Year's Eve, a wide plume of BB aerosol with large values of AAI (higher than 12) is transported toward the Tasman Sea on 1st January 2020 (Fig. 1a). Figure 1b depicts the CALIOP attenuated scattering ratio (SR) profiles on 1st January 2020 above New-Zealand. The CALIOP attenuated SR profiles are calculated along the CALIOP track (blue line in Fig. 1a) crossing the absorbing aerosol plume. CALIOP observations reveal a broad region of high values (ranging from 10 to 25) between 36° S and 46°S centered at 16.5 km altitude (Fig. 1b).

Figure 2a illustrates the daily extinction profiles at 532 nm derived from lidar measurements over Lauder (New-Zealand) between 1st December 2019 and 1st April 2020. Note that a strong convective activity prevented lidar operations between mid-December 2019 and the 1st January 2020. Figure 2a reveals a sharp increase in the extinction in the stratosphere over Lauder starting from mid-January 2020 with values ranging from 3 × 10^{-3} km^{-1} to 9 × 10^{-3} km^{-1}, one order of magnitude above the typical stratospheric aerosol background (Vernier et al., 2012). The vertical extent of the plume increased significantly between mid-January and 1st April 2020 with an aerosol layer spanning from 11.5 to 20

km. The ascent of the aerosol plume could be attributed to efficient adiabatic heating as a result of the strong absorption of solar radiation by this black carbon rich plume. Figure 2b depicts the daily evolution of CO mixing ratio profile obtained from FTIR measurements over Lauder between 1st December 2019 and 1st April 2020. Prior to the convective period, the maximum of CO mixing ratio (120-130 ppbv) is observed in the troposphere. An increase of CO mixing ratio in the lower stratosphere is visible from mid-December 2019. One can observe that the maximum of the CO mixing ratio (50-90 ppbv) is mainly observed in the UT-LS (9-13 km) during the February-April 2020 period. This could be explained by the fact that CO decays quickly due to photochemical oxidation whose efficiency increase with altitude.

The injection of BB aerosols and CO in the stratosphere induced significant disturbance evident in the total columns over Lauder (Fig. 3a). Figure 3a depicts the monthly mean evolution of AOD and total columns of CO (TCO) at Lauder between 1st December 2019 and 1st April 2020 obtained from sky-radiometer and FTIR measurements, respectively. AOD reaches its maximum value (0.17, 3 times higher than background value) in January 2020, decreasing to background values in February 2020 (Fig. 3a). The similar evolution is also observed for the TCO values. An abrupt increase in TCO (~9 % of the pre-event levels) is observed in January 2020 and the return to pre-event values is observed as of February 2020 as already shown in Kloss et al. (2021). Conversely, the perturbation on the stratospheric columns still persisting after February 2020. Figure 3b illustrates the monthly mean evolution of stratospheric AOD (sAOD) and CO (sCO) columns at Lauder between 1st December 2019 and 1st April 2020. The sAOD and sCO are calculated between 12 and 30 km from lidar and FTIR measurements, respectively. The evolution of sAOD and sCO is fairly similar (Fig. 3b). A statistically significant increase of sAOD is observed in January 2020 (2.5 times higher than background value) and still visible in April 2020 with same amplitude. sCO reaches its maximum values (~24 % of the pre-event levels) in January 2020 and slightly decreases in April 2020 (~14% of the pre-event).

Our works suggest that the injection of CO and absorbent aerosols ends up de-correlated in space and altitude given their different properties. In order to extend the discussion, the spatial dispersion of the Australian BB plume in the Southern Hemisphere will be discussed in the section.

4. Presence of the Australian BB plume over the SWIO basin

4.1 Aerosol and CO variability over a subtropical site: Reunion

Figure 4 depicts a time-averaged map of partial columns of aerosols (between 15 and 30 km, sAOD) and CO (between 9 and 30 km) respectively obtained from OMPS and IASI observations between 9th and 16th January 2020. The transport of the aerosol (with values ranging from 6 × 10^{-3} to 1 × 10^{-2} km^{-1}) and CO (with values ranging from 6 to 8 × 10^{17} molecules. cm^{-2}) plume over the Southern Pacific occurred mainly within the 18°S–60°S latitudinal band. One can observe an aerosol band (with values ranging from 5 × 10^{-3} to 9 × 10^{-3} km^{-1}) across the Southern Hemisphere between 40°S and 60°S during the 9-16th January 2020 period (Figure 4a). The Australian aerosol plume has already circled the Southern Hemisphere during the first two weeks of January 2020. The same conclusion cannot be made for CO from space-borne observations (Figure 4b). One can observe weak values of CO (less than 5 × 10^{17} molecule.cm^{-2}) over southern Atlantic and without real link with the large plume observed over southern Pacific (Fig. 4b).

Figure 5a depicts the evolution of the sAOD at 532 nm calculated between 15 and 30 km from the ground-based lidars (LiO3T and LiO3S) and OMPS observations over Reunion from 1st January to 1st March 2020. The Angström exponent for the 532–745 nm wavelength pair is adopted from methodology in Taha et al. (2021) and set to 1.9. Lidar observations over Reunion are also used to calculate the aerosol Angstrom exponent (using 355 nm and 532 nm pairs). An abrupt increase in the aerosol loading is clearly observed over Reunion as of 16th January 2020 according to satellite observations. This increase of the aerosol loading, three times above the typical background, was still visible until 1st March 2020. It is worthwhile mentioning that the sAOD values observed between 16th January and 1st March 2020 are higher than those observed during the passage of the Calbuco plume over Reunion site, which did not exceed 0.013 (Bègue et al., 2017). The increase of sAOD in mid-January coincided with an increase of CO, as shown in Figure 5b based on the use of partial columns and CO abundance from IASI and FTIR at the same site and over the same period. The evolution of CO obtained from IASI and FTIR measurements correlate. The ground-based observations show that the CO abundance observed during this increased phase is on average 20% higher than the values observed during the background period (Fig. 5b). The evolutions of sAOD and CO observations in mid-January suggests that Reunion, and its surrounding, have been influenced by the transport of **the BB plume**.

Figures 6a and 6b illustrate the night-averaged extinction profiles at 355 nm derived from lidar measurements over Reunion on January and February 2020, respectively. The two first weeks of January 2020 are representative of the January typical background (shaded area), as

illustrated on 13th January 2020 (Fig. 6a). Conversely, the extinction profiles at the end of January 2020 (27th and 28th) are marked by a significant increase (4 times higher than the background values) located in the lower stratosphere between 16.8 and 18 km altitude (equivalent to potential temperature levels 380-404 K). One can observe that the structure of the extinction profile in the lower stratosphere has changed between these two days. On 28th January, the extinction profile exhibits a sudden increase at 17.4 km (~400 K) and quickly decreased afterwards to values observed the previous day (Fig. 6a). It is worthwhile mentioning that the values of extinction (10 to 17 $\times$ 10^{-3} km^{-1}) observed in the lower stratosphere on these two days are of the same order as those observed at Lauder a few days after the pyro-convective event (Fig. 2). Figure 6a also reveals a statistically significant increase (4 times higher than background values) in aerosol extinction between 15 and 16.5 km altitude (361-375 K), on 27th and 28th January 2020. Over Reunion, the lidar observations hence confirm the presence of a significant aerosol layer in the UT-LS by the end of January. In February, the extinction profiles clearly exhibit two significant aerosol layers with the first one located between 16 and 19.5 km (370-440 K) and the second one between 20 and 22.5 km (465-500 K) (Fig. 6b).

To further discuss the optical properties of these aerosol layers, the Angstrom exponent has been calculated between 355 nm and 532 nm from the LiO3S and LiO3T measurements (Figs. 6c and 6d). In February, the Angström exponent values reveal that the two aerosol layers consist mainly of small aerosol particles (Fig. 6d), consistent with a stratospheric smoke layer (Haarig et al., 2018; Hu et al., 2019; Ohneiser et al., 2021). In January, the profile of Angström exponent exhibits more variability in the UT-LS (Fig. 6c) with values ranging from 0.6 to 1.9, on 27th and 28th January. The wide range of Angström exponent values suggests that the aerosol layer is not homogeneously distributed at this stage and might be interpreted as a mixture of fresh and aged smoke layers (Fig. 6c). **Indeed, Muller et al, 2007 showed that ageing of transported smoke translates into a decreasing of the Angström exponent.** This may indicate growth and removal processes (e.g., coagulation, condensation, sedimentation) which can modulate the morphology and mixing state of the aerosol layer during its transport (Burton et al., 2015; Hamil et al., 1997). The residence time of the aerosol particles in the atmosphere depends on the balance between the growth processes and the removal processes, which are likely to be controlled by the dynamical context. Previous works showed that the dynamical context can modulate the structure and optical properties of the aerosol layer over a given site from day to day (Bègue et al., 2017; Kremser et al., 2016). Fresh aerosols can be rapidly transported and mixed with pre-existing aged aerosol. Given the fact that the Angström exponent values decrease with the duration of transport, we cannot exclude that the vertical

distribution of optical properties of aerosol over Reunion may also be explained by the regional transport of air masses.

4.2 Origin of the air masses

To analyze the origin of air masses at Reunion on 27th and 28th January, one-month backward trajectories **were** calculated using FLEXPART (Aliaga et al., 2021; Eckhardt et al., 2017; Xu et al., 2021). A period of one month **was** chosen because it refers to time separating the pyro-convective outbreak event and the day of the measurement at Reunion. The representation of the PES (potential emission sensitivity) from back-trajectories simulations initialized at 18 km originating from Reunion on 27th and 28th January 2020 are presented in Figure 7.

Figures 7A-1 and 7B-1 display the horizontal trajectory paths, whilst vertical movement is shown in Figures 7A-2 and 7B-2, respectively. The vertical transect of FLEXPART back trajectories in Figure 7A-2 confirms a high probability of air mass contribution from the Australia if the fires emissions are directly injected into the stratosphere by convection (black rectangle in the figure), (i.e. layer of 9 to 16 km of injection taken for the PES, see section 2.3.1). Then, according to FLEXPART results, the air masses at 18 km over Australia moved westward and reached Reunion on 27th January. One can observe that the same pattern is occured on 28th January 2020 (Figs. 7B-1 and 7B-2). One part of the Australian smoke layer is advected zonally by the prevailing easterly winds and is observed over Reunion on 27th and 28th January 2020 at 18 km. It is **worth** mentioning that the same pattern has been observed during the volcanic eruption of the Hunga Tonga on January 2022 (Baron et al, 2023, Kloss et al., 2022; Sellitto et al., 2022). The FLEXPART simulations also suggest that Reunion is also influenced by eastward transport of air masses. This pathway is clearly visible on 28th January 2020 (Figs. 7B-1 and 7B-2). Figure 7B-1 reveals that air masses coming from the South American region and Australia region both reach the SWIO basin by passing over southern Africa. Furthermore, air masses from high latitudes seem to cross the subtropical latitudes following a wave shape and reach the SWIO basin by passing over the Cape of Good Hope (Figure 7B-1).

In order to improve the discussion on this eastward transport of air masses over the SWIO basin, the MIMOSA model has been used to produce a continuous evolution of PV fields for the period from 1st to 31st January 2020. Two advected PV maps derived for the 400 K isentropic level from the MIMOSA model are depicted in Figure 8. The localization of the aerosol plume obtained from OMPS observations at the 400 K ± 5 K isentropic level are also superimposed (Fig. 8). The 400 K isentropic level is chosen according to the layers observed in the extinction profiles over Reunion between 390 and 404 K isentropic level on 27th and 28th January 2020

(Fig. 6a). Figure 8 reveals significant wave activity during these two days. It is clearly shown that air masses from mid-latitudes (40-60°S) cross the subtropical latitudes (20-40°S) and are advected eastward between South Africa and Madagascar following a wave shape. **Given the Australian BB aerosol are mainly located in the mid-latitudes (Fig. 4a), we can reasonably conclude that the filament reaching the SWIO basin contains aerosol from Australian BB event. On 27th January, air masses containing aerosol are observed at Madagascar and its surroundings (Fig. 8a). These air masses are advected eastward following the displacement of the wave shape and reach Reunion, on 28th January (Fig. 8b). Parts of the smoke plume underwent an isentropic transport from the mid to tropical latitudes following two distinct pathways to reach Reunion.**

Nevertheless, the contribution of the Australian BB event on the variability of **aerosol** in the upper troposphere (15-16.5 km; 361-375 K) remains ambiguous. The representation of the PES from back-trajectories simulations initialized at 16 km originating from Reunion for the 27th and 28th January 2020 are presented in Figure 9. Figure 9A-1 and 9B-1 reveal that the trajectories from Reunion at 16 km pass over southern Africa and Madagascar. One can observe that the highest values of PES are located over southern Africa and Madagascar (Figs. 9A-1 and 9B-1). Furthermore, the FLEXPART simulations suggest that air masses from southern Africa and Madagascar might have reached altitudes up to 16 km between 25°E and 55°E in longitude and reached Reunion on 27th and 28th January 2020 (Figs. 9A-2 and 9A-2). The results of Figure 9 show an influence of air masses coming from Africa and reaching the SWIO basin at 16 km. Thus, the moderate increase in aerosol extinction observed in the upper troposphere (between 16 and 17 km altitude) on 27th and 28th January in Figure 6a may be attributed to air masses from regional sources, namely southern Africa and Madagascar.

In summary, our analysis suggests that the variability of CO and aerosols in the UT-LS over the SWIO basin in January is explained both by long-range and regional transport of air masses. The extent to which regional sources have contributed to the variability of the atmospheric compounds over the SWIO is now investigated.

5. Discussion on the influence of the regional sources versus long range transport sources

We investigate the contribution of the African and Australian BB activity on the atmospheric composition in the UT-LS over the SWIO basin. Because a significant simultaneous increase of CO and sAOD is observed over Reunion and its surroundings from 16th to 29th January 2020, the discussion will focus on this period. In order to assess the contribution of African and Australian BB activity, FLEXPART is coupled with the GFAS inventory.

5.1 Presence of African air masses in the UT-LS

The location of fire-flagged pixels and the associated Fire Radiation Power (FRP) values from MODIS between 16th and 29th January 2020 are reported in Figure 10a. FRP gives quantitative information on combustion rates and its intensity. The sparse activity of the African fires in January is clearly illustrated in Figure 10a with moderate values of FRP ranging from 20 to 200 MW.m^{-2}. These values are ten times lower than those observed over the southeastern Australia between 30th December 2019 and 12th January 2020 (Bègue et al., 2021). One can observe that the African BB activity in January 2020 is mainly located over the northwestern (near the Equator) and southeastern side of southern Africa. The most intense values (100-200 MW.m^{-2}) are observed over the southeastern side.

Despite this sparse activity of BB, the amount of CO injected into the atmosphere is fairly significant, ranging from 5 to 6 × 10^{17} molecules.cm^{-2}. A Time-averaged map of the partial column of CO (between 9 and 30 km) from IASI observations between 16th and 29th January 2020 over the SWIO basin is reported on Figure 10b. The partial column of CO over the southern Africa is characterized by two regions of high values (higher than 5 × 10^{17} molecules.cm^{-2}). The first region stretches between the eastern side of southern Africa and western side of Madagascar which corresponds to a domain extending between 10°S and 25°S in latitude and 30°E and 45°E in longitude (Fig. 10b). The second region is located on the opposite side, over a domain extending between 10°S and 15°S in latitude and 5°E and 15°E in longitude.

Figure 10c depicts a time-averaged map of OLR (Outgoing Longwave Radiation) anomalies from NCEP analysis between 16th and 29th January 2020. One can observe that the main convective regions (region of negative OLR anomalies) are located in mainland Africa between 12° S and 25° S and the northern side of the SWIO basin. It is worthwhile mentioning that the daily brightness temperature values obtained from MODIS between 16th and 29th January 2020 (not shown) are ranging from 195 to 210 K over the eastern side of southern Africa and the Mozambique Channel (around the north tip of Madagascar). These values of brightness temperature can be attributed to deep convection clouds (Héron et al., 2020; Young et al., 2013). Through the analysis of ERA-Interim data over a period of 66 years, Lashkari et al. (2017) investigated the annual and seasonal displacement of the ITCZ. On average, the motion of ITCZ over southern Africa on January is characterized by southward move from 5°N to 20°S in latitude occurring between 20° E and 35° E in longitude (Fig 10a; Lashkari et al., 2017). Over the

Mozambique Channel, the deep convection can be explained by the tropical storm activity. Indeed, a tropical depression has been formed in the east side of the Mozambique Channel (near the northwestern side of Madagascar) between 20th and 22nd January 2020. This tropical depression reached the stage of strong tropical storm on 24th January 2020 and was called Diane by the RMSC of Reunion. The intensification of the tropical depression into strong tropical storm occurred around the north tip of Madagascar. Diane passed near Reunion on 25th January 2020 (Fig. 10c). In the present study, the convective activity over southern Africa and the SWIO basin may hence be due to both ITCZ proximity and Diane activity.

To further discuss the vertical distribution of CO in the UT-LS within the region of deep convection, the vertical cross section of CO and water vapor mixing ratio anomalies calculated from MLS observations between 16th to 29th January 2020 are analyzed (Figs. 11a and 11b). The CO and water vapor mixing ratio anomalies are calculated as a relative difference by considering the monthly background means as the reference values. The calculations are performed over a domain extending between 10°S and 25°S in latitude and 30°E and 60°E in longitude (black box in Fig. 10b). The altitude-longitude cross-section is averaged for all latitudes covering the study domain. This domain includes both the region of deep convection and the first region of high values of CO. The monthly background is calculated from available MLS observations in January between 2017 and 2019. Figure 11a exhibits two regions of high values of CO mixing ratio anomalies (higher than 15%) centered at 37°E and 50°E in longitude. The maximum CO mixing ratio anomalies in the first region are centered at 215 hPa (~12 km) with anomalies ranging from 25% to 30%. The values of the anomalies decreased rapidly with altitude. Indeed, the anomalies values obtained at 146 hPa (~15 km) and 100 hPa (~17 km) ranged from 20% to 25% and from 15% to 20 %, respectively. In the second region, the maximum CO mixing ratio anomalies are also centered in the middle troposphere (215 hPa). One can observe that these regions of CO mixing ratio anomalies are in coincidence with two regions of high values (higher than 20%) of water vapor mixing anomalies (Fig. 11b). The maxima of water vapor mixing ratio anomalies are centered at 146 hPa with values ranging from 40% to 50%. We can assume that the convective activity induced by Diane near Madagascar may have contributed to lift air masses enriched in CO from the lower troposphere. This is consistent with the FLEXPART simulations which highlight a lift of air masses from the lower troposphere to lower stratosphere between 25°E to 55° E in longitude (Figure 9). One can observe that the most significant anomalies of the vertical

distribution of CO and water vapor mixing ratio stretch from the middle troposphere (215 hPa) up to the tropopause layer (100 hPa,). At 68 hPa, it can be observed that high values of water vapor mixing ratio anomalies are not in coincidence with high values of CO mixing ratio anomalies, but located along the vertical extent of the maxima of CO mixing ratio anomalies in the troposphere.

Our analysis corroborates the results found by Héron et al. (2020). Based on radiosonde and satellite observations, Héron et al. (2020) showed that convective activity over the SWIO basin has the potential to influence the variability of ozone and water vapor in the upper-troposphere during the austral summer. Our results demonstrate that the variability of CO and aerosol over the SWIO basin can be explained both by the influence of long-range transport of the Australian fires plumes, together with regional transport from southern Africa, enhanced by convective activity due to the passage of a tropical storm.

5.2 Discussion on the variability of the total and partial column of CO

The evolutions of the total and partial column of CO observed by IASI and simulated by FLEXPART from 15th to 29th January over Reunion are depicted in Figure 12a. Despite the underestimation of the simulated total and partial column of CO, their overall temporal evolution is fairly well reproduced by FLEXPART (Fig. 12a). **The BB contributions on the vertical distribution of CO are calculated by combining the PES with an emission inventory. A mass concentration profile of CO is extracted by summing all the output grid-points.** The discrepancies between FLEXPART and IASI may be attributable to several possible caveats. **One** possible source of error can be the fact that the vertical motion induced by pyro-convection is not included in FLEXPART. We **test** this issue by applying an injection height in agreement with CALIOP observations (9-16 km, Fig. 1) for the Australian plume (Khaykin et al., 2020). An injection height ranging up to 3 km was chosen for the African fires (Labonne et al., 2007). The injection height of the plume plays a key role in its long-range transport (Sofiev et al., 2012). An inappropriate or unrealistic injection height can lead to either a dilution or an overestimation of the plume. The injection height depends on the intensity of the fire, as well as on the meteorological conditions. Another possible explanation in these differences can come from the duration of the backward calculation (1 month) (Brocchi et al., 2018). Underestimation of the partial columns of CO may also be the result of an underestimation of the CO emissions by GFAS. In the framework of their FLEXPART simulation, Brocchi et al. (2018) reveal that an amplification factor of **two** has been applied to CO emissions from GFAS to get similar CO quantities to observations.

Nevertheless, these simulations can reasonably be used to discuss the contribution of CO emissions from Africa and Australia on the variability of the total and partial columns of CO over the SWIO basin. The contribution of the CO emissions from Africa and Australia **to** the partial columns of CO over Reunion is isolated and depicted in Figure 12. On average, the CO emissions from Africa contribute up to 90% of the enhancement of the partial column of CO from 15th to 29th January. The transport of the CO plume induced by the Australian sources **has** not been efficient over the SWIO basin. The variability of CO over the SWIO basin is hence mainly explained by the regional transport of air masses.

5.3 Discussion on the variability of the aerosols

The FLEXPART simulations for the contribution of aerosol (BC and OC) emissions from Africa and Australia on the sAOD over Reunion use the same parameters as for CO, in particular the injection height. Figure 12b depicts the evolution of the sAOD observed by OMPS and simulated by FLEXPART from 15th to 29th January over Reunion. Unfortunately, few data have been recorded during the period aforementioned. Nevertheless, the simulated sAOD compare fairly well with the available OMPS observations during this period, and the sAOD peak observed on 19th January is acceptably well reproduced. On average, the aerosol emissions from Australia contributed up to 95 % of the sAOD variability over Reunion from 15th to 29th January (Fig. 12b). **The** evolution of sAOD is not correlated to the evolution of the aerosol emission from Africa**,** which is marked by an increase from 21st to 29th January. The weak contribution of African component on the sAOD can be explained by the fact that the amounts of African BB aerosols injected in the atmosphere by the convective activity decrease with altitude. Moreover, it is likely that aerosol would be scavenged by cloud droplets (**a process** taken into account in FLEXPART) in a strongly convective environment such as tropical storm Diane. Overall, FLEXPART simulations clearly suggested the contribution of African and Australian BB aerosols.

6. Summary and Conclusion

The complex aerosol and CO variabilities over the SWIO basin during the 2020 austral summer have been investigated. The meteorological context and the extensive fires over southeastern Australia were favorable **for triggering** pyro-convective events between 29th December 2019 and 12th January 2020. These pyro-convective events led to massive injection of combustion products in the stratosphere. The ground-based and space-borne lidars revealed the presence of an intense stratospheric **aerosol** layer over the southeastern Australia region. Over the Lauder site in New Zealand, this smoke layer was detected in the stratosphere (centered at 16 km) until April and beyond. The analysis of the spatial and temporal dispersion of **the Australian BB**

plume highlighted its quick transport circling the entire Southern Hemisphere in less than two weeks. Furthermore, the satellite observations revealed that the transport of the Australian smoke layer has been mainly bounded within an extra-tropical latitudinal band.

Nevertheless, the numerical models clearly showed the influence of the Australian smoke layer on the variability of aerosol over the SWIO basin. Over Reunion, the aerosol extinction profiles exhibited a significant increase in the lower stratosphere during the end of January. The MIMOSA simulations highlighted the isentropic transport of **the Australian BB aerosol** from extra-tropical latitudes to Reunion at 400 K isentropic level, on 28th January. As a consequence, the corresponding aerosol extinction profile exhibited a sudden increase by drawing a structure similar to a laminae at the 400 K isentropic level. The aerosol extinction profiles also exhibited a moderate increase in the upper troposphere.

This paper investigates for the first time the possibility of the African emissions from BB to influence the CO and aerosol distribution in the UT-LS during the convective season. Despite the fact that African BB activity is usually sparse in January, it contributed to **modulation of** the vertical distribution of CO and aerosols in the upper troposphere over the SWIO basin. The analysis of satellite observations and FLEXPART simulations **suggests** that**,** because of the convective activity, air masses enriched in CO and aerosols have been lifted from the lower troposphere to the lower stratosphere. Air masses from Africa contributed up to 90% of the total and partial column (between 9 and 30 km) of CO variability over Reunion and its surroundings. The simulations shows that the modulation of the aerosol extinction in the upper troposphere and the lower stratosphere, over Reunion, was driven by the transport of air masses from both Africa and Australia, respectively. Our findings suggest simultaneous presence of African and Australian aerosol smoke layers at Reunion.

Acknowledgements

Data used in this publication were obtained from NDACC network and are available through its website (http://www.ndacc.org/). The work of S. Khaykin has been supported by the Agence Nationale de la Recherche PyroStrat project (21-CE01- 335 0007-01). IASI was developed and built under the responsibility of the “Centre National d’Etudes Spatiales” (CNES, France) and flown on board the MetOp satellites as part of the EUMETSAT Polar System. The authors thank the AERIS infrastructure (https://iasi.aeris-data.fr/) for providing access to the IASI data, the National Aeronautical and Space Administration (NASA) for providing CALIOP data, MLS and MODIS fire products. We would especially like to thank the staff of the team working on the lidar systems at the Maïdo observatory. The French Research Infrastructure ACTRIS-FR, CNES and the EU project REALISTIC (GA 101086690) are also acknowledged for their

support in the upgrade and operation of the Maïdo observatory lidars. Lauder observations are funded by the New Zealand Government's Strategic Science Investment Fund (SSIF), administered by the Ministry of Business, Innovation and Employment (MBIE). The TCCON site at Réunion Island has been operated by the Royal Belgian Institute for Space Aeronomy with financial support since 2014 by the EU project ICOS-Inwire, the ministerial decree for ICOS (FR/35/IC1 to FR/35/C6), ESFRI-FED ICOS-BE project and local activities supported by LACy/UMR8105 and by OSU-R/UMS3365 – Université de La Réunion. The lidar measurements are supported **by funding from** GOSAT series project.

Data availability

The data used for this study are available and open access by request to scientist mentioned or through the link hereafter: Lidar measurements (tetsu@mri-jma.go.jp, nelson.begue@univ-reunion.fr), FTIR measurements from TCCON network (mahesh.sha@aeronomie.be); Lauder FTIR data available on the NDACC public access database (https://www-air.larc.nasa.gov/missions/ndacc/data.html); The satellite observations and emission inventory used are available on-line from the sources as stated in the manuscript.

Authors contributions

Conceptualization, N.B.; methodology and software, N.B, A.B. and G.K.; validation and data curation, N.B., A.B, GK., S.K, C.C., P.C., D.S., J.R., R.Q, B.R, S.T and P.S.; original draft preparation and writing, N.B.; All authors have read and agreed to the published version of the manuscript.

REFRENCES

Aliaga, D., Sinclair, V. A., Andrade, M., Artaxo, P., Carbone, S., Kadantsev, E and Bianchi, F.: Identifying source regions of air masses sampled at the tropical high-altitude site of Chacaltaya using WRF-FLEXPART and cluster analysis. Atmospheric Chemistry and Physics, 21(21), 16453-16477, 2021

Andreae, M. O and Merlet, P.: Emission of trace gases and aerosols from biomass burning. Global biogeochemical cycles, 15(4), 955-966, 2001

Baray, J.-L., Courcoux, Y., Keckhut, P., Portafaix, T., Tulet, P., Cammas, J.-P., Hauchecorne, A., Godin Beekmann, S., De Mazière, M., Hermans, C., Desmet, F., Sellegri, K., Colomb, A., Ramonet, M., Sciare, J., Vuillemin, C., Hoareau, C., Dionisi, D., Duflot, V., Vérèmes, H., Porteneuve, J., Gabarrot, F., Gaudo, T., Metzger, J.-M., Payen, G., Leclair de Bellevue, J., Barthe, C., Posny, F., Ricaud, P., Abchiche, A., and Delmas, R.: Maïdo observatory: a new high-altitude station facility at Reunion Island (21° S, 55° E) for long-term atmospheric remote sensing and in situ measurements, Atmos. Meas. Tech., 6, 2865–2877, https://doi.org/10.5194/amt-6-2865-2013, 2013

Baray, J.-L., Leveau, J., Baldy, S., Jouzel, J., Keckhut, P., Bergametti, G., Ancellet, G., Bencherif, H., Cadet, B., Carleer, M., David, C., De Mazière, M., Faduilhe, D., Godin-Beekmann, S., Goloub, P., Goutail, F., Metzger, J.-M., Morel, B., Pommereau, J.-P., Porteneuve, J., Portafaix, T., Posny, F., ROBERT, L., and Van Roozendael, M.: An instrumented station for the survey of ozone and climate change in the southern tropics, 8, 1020–1028, https://doi.org/10.1039/b607762e, 2006.

Barimalala, R., Desbiolles, F., Blamey, R. C., & Reason, C.: Madagascar influence on the South Indian Ocean Convergence Zone, the Mozambique Channel Trough and southern African rainfall. Geophysical Research Letters, 45, 11,380–11,389. https://doi.org/10.1029/ 2018GL079964, 2018

Baron, A., Chazette, P., Khaykin, S., Payen, G., Marquestaut, N., Bègue, N. and Duflot, V.: Early Evolution of the Stratospheric Aerosol Plume Following the 2022 Hunga Tonga-Hunga Ha'apai Eruption: Lidar Observations From Reunion (21° S, 55° E). Geophysical Research Letters, 50(10), https://doi.org/10.1029/2022GL101751, e2022GL101751, 2023

Barthe, C., Bousquet, O., Bielli, S., Tulet, P., Pianezze, J., Claeys, M. and Zucule, J.: Impact of tropical cyclones on inhabited areas of the swio basin at present and future horizons. part 2:

Modeling component of the research program renovrisk-cyclone. Atmosphere, 12(6), 689, 2021

Bègue, N., Bencherif, H., Jegou, F., Vérèmes, H., Khaykin, S., Krysztofiak, G., Portafaix, T., Duflot, V., Baron, A., Berthet, G., Kloss, C., Payen, G., Keckhut, P., Coheur, P-F., Clerbeaux, C., Smale, D., Robinson, J., Querel, R and Smale, P. : Transport and variability of tropospheric ozone over Oceania and southern pacific during the 2019–20 Australian bushfires. Remote Sensing, 13(16), 3092, 2021

Bègue, N., Vignelles, D., Berthet, G., Portafaix, T., Payen, G., Jégou, F., Bencherif, H., Jumelet, J., Vernier, J. P., Lurton., T., Renard, J. B., Clarisse., L., Duverger, V., Posny, F., Metzger, J. M., and Godin-Beekmann, S.: Long-range isentropic transport of stratospheric aerosols over Southern Hemisphere following the Calbuco eruption in April 2015, 15019–15036, https://doi.org/10.5194/acp-17-15019-2017, 2017.

Bencherif, H., Bègue, N., Kirsch Pinheiro, D., Du Preez, D. J., Cadet, J. M., da Silva Lopes, F. J. and Clerbaux, C.: Investigating the long-range transport of aerosol plumes following the Amazon fires (August 2019): a multi-instrumental approach from ground-based and satellite observations. Remote Sensing, 12(22), 3846, 2020

Bencherif, H., El Amraoui, L., Kirgis, G., Leclair De Bellevue, J., Hauchecorne, A., Mzé, N., Portafaix, T., Pazmino, A., and Goutail, F.: Analysis of a rapid increase of stratospheric ozone during late austral summer 2008 over Kerguelen (49.4° S, 70.3° E), Atmos. Chem. Phys., 11, 363–373, https://doi.org/10.5194/acp-11-363-2011, 2011

Boers, R., A. T. de Laat, D. C. Stein Zweers, and R. J. Dirksen: Lifting potential of solar-heated aerosol layers, Geophys. Res. Lett., 37, L24802, doi:10.1029/2010GL045171, 2010

Burton, S.P., Hair, J.W., Kahnert, M., Ferrare, R.A., Hostetler, C.A., Cook, A.L., Harper, D.B., Berkoff, T.A., Seaman, S.T., Collins, J.E., Fenn, M.A., Rogers, R.R., 2015. Observations of the spectral dependence of linear particle depolarization ratio of aerosols using NASA Langley airborne High Spectral Resolution Lidar. Atmos. Chem. Phys. 15, 13453–13473. https://doi.org/10.5194/acp-15-13453-2015

Cai, D., Abram, N. J., Sharples, J. J. and Perkins-Kirkpatrick, S. E. (2022). Increasing intensity and frequency of cold fronts contributed to Australia's 2019–2020 Black Summer fire disaster. Environmental Research Letters, 17(9), 094044.

Campanelli, M., Estelles, V., Tomasi, C., Nakajima, T., Malvestuto, V., and Martinez-Lozano, J. A.: Application of the SKYRAD improved Langley plot method for the in-situ calibration of CIMEL sun-sky photometers, Appl. Optics, 46, 2688–2702, 2007.

Che, H., Shi, G., Uchiyama, A., Yamazaki, A., Chen, H., Goloub, P., and Zhang, X.: Intercomparison between aerosol optical properties by a PREDE skyradiometer and CIMEL sunphotometer over Beijing, China, Atmos. Chem. Phys., 8, 3199–3214, doi:10.5194/acp-8-3199-2008, 2008.

Clain, G., Baray, J. L., Delmas, R., Diab, R., Leclair de Bellevue, J., Keckhut, P., Posny, F., Metzger, J. M., and Cammas, J. P.: Tropospheric ozone climatology at two Southern Hemisphere tropical/subtropical sites, (Reunion Island and Irene, South Africa) from ozonesondes, LIDAR, and in situ aircraft measurements, 9, Atmos. Chem. Phys., 1723–1734, https://doi.org/10.5194/acp-9-1723-2009, 2009

Clerbaux, C., Boynard, A., Clarisse, L., George, M., Hadji-Lazaro, J., Herbin, H., Hurtmans, D., Pommier, M., Razavi, A., Turquety, S: Monitoring of atmospheric composition using the thermal infrared IASI/MetOp sounder, Atmos. Chem. Phys. 2009, 9, 6041–6054, 2009.

Coheur, P.-F., Clarisse, L., Turquety, S., Hurtmans, D., and Clerbaux, C.: IASI measurements of reactive trace species in BB plumes, Atmos. Chem. Phys., 9, 5655–5667, doi:10.5194/acp-9-5655-2009, 2009.

Darbyshire, E., Morgan, W. T., Allan, J. D., Liu, D., Flynn, M. J., Dorsey, J. R and Coe, H: The vertical distribution of biomass burning pollution over tropical South America from aircraft in situ measurements during SAMBBA. Atmospheric Chemistry and Physics, 19(9), 5771-5790, 2019

De Laat, A.T.J.; Stein Zweers, D.C.; Boers, R.; Tuinder, O.N. A solar escalator: Observational evidence of the self-lifting of smoke and aerosols by absorption of solar radiation in the February 2009 Australian Black Saturday plume. J. Geophys. Res. Atmos. 2012, 117.

Dowdy, A. J and Pepler, A: Pyroconvection risk in Australia: Climatological changes in atmospheric stability and surface fire weather conditions. Geophysical Research Letters, 45, 2005–2013. https://doi.org/10.1002/2017GL076654, 2018

De Mazière, M., Sha, M. K., Desmet, F., Hermans, C., Scolas, F., Kumps, N., Metzger, J.-M., Duflot, V., and Cammas, J.-P.: TCOON data from Réunion Island 5RE), Release GG2014.R1, Version R1, CaltechDATA [data set], https://doi.org/10.14291/TCCON.GGG2014.REUNION01.R1, 2017

Duflot, V., Dils, B., Baray, J. L., De Mazière, M., Attié, J. L., Vanhaelewyn, G and Delmas, R.: Analysis of the origin of the distribution of CO in the subtropical southern Indian Ocean in 2007. Journal of Geophysical Research: Atmospheres, 115(D22), 2010

Duflot, V., Royer, P., Chazette, P., Baray, J. L., Courcoux, Y. and Delmas, R.: Marine and BB aerosols in the southern Indian Ocean: Retrieval of aerosol optical properties from shipborne lidar and Sun photometer measurements. Journal of Geophysical Research: Atmospheres, 116(D18), 2011

Duflot, V., Bègue, N., Pouliquen, M. L., Goloub, P. and Metzger, J. M : Aerosols on the Tropical Island of La Réunion (21° S, 55° E): Assessment of Climatology, Origin of Variability and Trend. Remote Sensing, 14(19), 4945, 2022

Edwards, D. P., Emmons, L. K., Gille, J. C., Chu, A., Attié, J. L., Giglio, L and Drummond, J. R.: Satellite-observed pollution from Southern Hemisphere biomass burning. Journal of Geophysical Research: Atmospheres, 111(D14), 2006

Fromm, M., Lindsey, D. T., Servranckx, R., Yue, G., Trickl, T., Sica, R.: The untold story of pyro-cumulonimbus. Bulletin of the American Meteorological Society, 91(9), 2010

Hamill, P., Jensen, E. J., Russell, P. B., and Bauman, J. J.: The life cycle of stratospheric aerosol particles, B. Am. Meteorol. Soc., 78, 1395–1410, https://doi.org/10.1175/1520-0477(1997)078E2.0.CO;2, 1997

Garstang, M., Tyson, P. D., Browell, E. and Swap, R. J.: . Large scale transport of biogenic and biomass burning products. JS Levine, 389-395, 1996

Haarig, M.; Ansmann, A.; Baars, H.; Jimenez, C.; Veselovskii, I.; Engelmann, R.; Althausen, D. Depolarization and lidar ratios at 355, 532, and 1064 nm and microphysical properties of aged tropospheric and stratospheric Canadian wildfire smoke. Atmos. Chem. Phys. 2018, 18, 11847–11861.

Hashimoto, M., Nakajima, T., Dubovik, O., Campanelli, M., Che, H., Khatri, P., Takamura, T and Pandithurai, G: Development of a new data-processing method for SKYNET sky radiometer observations. Atmospheric Measurement Techniques, 5(11), 2723-2737, 2012

Hauchecorne, A., Godin, S., Marchand, M., Heese, B., and Souprayen, C.: Quantification of the transport of chemical constituents from the polar vortex to midlatitudes in the lower stratosphere using the high-resolution advection model MIMOSA and effective diffusivity, J. Geophys. Res.-Atmos., 107, 1–13, 2002

Héron, D., Evan, S., Brioude, J., Rosenlof, K., Posny, F., Metzger, J. M., & Cammas, J. P.: Impact of convection on the upper-tropospheric composition (water vapor and ozone) over a subtropical site (Réunion island; 21.1° S, 55.5° E) in the Indian Ocean. Atmospheric Chemistry and Physics, 20(14), 8611-8626., 2020

Heese, B., Godin, S., and Hauchecorne, A.: Airborne lidar measurements of ozone filaments during METRO–A validation of PV advection model MIMOSA, J. Geophys. Res, 106, 20011–20024, 2001.

Holanda, B. A., Pöhlker, M. L., Walter, D., Saturno, J., Sörgel, M., Ditas, J and Pöhlker, C: Influx of African biomass burning aerosol during the Amazonian dry season through layered transatlantic transport of black carbon-rich smoke. Atmospheric Chemistry and Physics, 20(8), 4757-4785, 2020

Hu, Q., Goloub, P., Veselovskii, I., Bravo-Aranda, J.-A., Popovici, I. E., Podvin, T., Haeffelin, M., Lopatin, A., Dubovik, O., Pietras, C., Huang, X., Torres, B., and Chen, C.: Long-range-transported Canadian smoke plumes in the lower stratosphere over northern France, Atmos. Chem. Phys., 19, 1173–1193, https://doi.org/10.5194/acp-19-1173-2019, 2019.

Hurtmans, D., Coheur, P.F.; Wespes, C., Clarisse, L., Scharf, O., Clerbaux, C., Hadji-Lazaro, J., George, M., Turquety, S: FORLI radiative transfer and retrieval code for IASI. J. Quant. Spectrosc. Radiat. Transf. 2012, 113, 1391–1408, 2012

Jäger, H. and Deshler, T.: Lidar backscatter to extinction, mass and area conversions for stratospheric aerosols based on midlatitude balloon borne size distribution measurements, Geophys. Res. Lett., 29, 1929, https://doi.org/10.1029/2002GL015609, 2002

Jones, N. B., Rinsland, C. P., Liley, J. B., and Rosen, J.: Correlation of aerosol and carbon monoxide at 45 S: Evidence of BB emissions. Geophysical research letters, 28(4), 709-712., 2001

Kablick III, G. P., Allen, D. R., Fromm, M. D. and Nedoluha, G. E: Australian pyroCb smoke generates synoptic-scale stratospheric anticyclones, Geophys. Res. Let., 47(13), e2020GL088101, 2020.

Khaykin, S., Legras, B., Bucci, S., Sellitto, P., Isaksen, L., Tence, F. and Godin-Beekmann, S: The 2019/20 Australian wildfires generated a persistent smoke-charged vortex rising up to 35 km altitude. Communications Earth & Environment, 1(1), 1-12, 2020.

Khaykin, S. M., Godin-Beekmann, S., Hauchecorne, A., Pelon, J., Ravetta, F., and Keckhut, P: Stratospheric smoke with unprecedentedly high backscatter observed by lidars above southern France, Geophys. Res. Lett., 1944, 8007, doi:10.1002/2017GL076763, 2018.

Kaufman, Y. J., Ichoku, C., Giglio, L., Korontzi, S., Chu, D. A., Hao, W. M and Justice, C. O.: Fire and smoke observed from the Earth Observing System MODIS instrument--

products, validation, and operational use. International Journal of Remote Sensing, 24(8), 1765-1781, 2003

Klett, J. D.: Lidar inversion with variable backscatter/extinction ratios, Appl. Opt., AO, 24, 1638–1643, https://doi.org/10.1364/AO.24.001638, 1985.

Kloss, C.; Sellitto, P., Von Hobe, M.; Berthet, G.; Smale, D.; Krysztofiak, G.; Legras, B. Australian fires 2019–2020: Tropospheric and stratospheric pollution throughout the whole fire season. Front. Environ. Sci. 2021, 9, 220, 2021

Kloss, C., Berthet, G., Sellitto, P., Ploeger, F., Bucci, S., Khaykin, S., Jégou, F., Taha, G., Thomason, L. W., Barret, B., Le Flochmoen, E., von Hobe, M., Bossolasco, A., Bègue, N., and Legras, B.: Transport of the 2017 Canadian wildfire plume to the tropics via the Asian monsoon circulation, Atmos. Chem. Phys., 19, 13547–13567, https://doi.org/10.5194/acp-19-13547-2019, 2019.

Kloss, C., Sellitto, P., Renard, J. B., Baron, A., Bègue, N., Legras, B., Berthet., G., Briaud., E., Carboni., E., Duchamp., C., Duflot., V., Jacquet., P., Marquestaut., N., Metzger. J-M., Payen., G., Ranaivombola., M., Roberts., T., Siddans., R. and Jegou, F.: Aerosol characterization of the stratospheric plume from the volcanic eruption at Hunga Tonga 15 January 2022. Geophysical Research Letters, 49(16), e2022GL099394., 2022

Kremser, S., Thomason, L. W., Hobe, M., et al.: Stratospheric aerosol – Observations, processes, and impact on climate, Rev. Geophys., 54, 278–335, 2016.

Labonne, M., Bréon, F. M and Chevallier, F.: Injection height of BB aerosols as seen from a Lashkari, H., Mohammadi, Z., & Keikhosravi, G.: Annual fluctuations and displacements of inter tropical convergence zone (ITCZ) within the range of Atlantic Ocean-India. Open Journal of Ecology, 7(1), 12-33.spaceborne lidar. Geophysical Research Letters, 34(11), 2017

Levin, N., Yebra, M. and Phinn, S.: Unveiling the factors responsible for Australia's Black Summer fires of 2019/2020. Fire, 4(3), 58, 2021

Livesey, N., Read, W., Wagner, P., Froidevaux, L., Santee, M., Schwartz, M., et al.: Earth Observing System (EOS): Aura Microwave Limb Sounder (MLS): Version 5.0x Level 2 and 3 Data Quality and Description Document. Jet Propulsion Lab. JPL. D-105336 Rev. A, 2020

de Mazière, M. D., Thompson, A. M., Kurylo, M. J., Wild, J. D., Bernhard, G., Blumenstock, T. and Strahan, S. E: The Network for the Detection of Atmospheric Composition Change (NDACC): history, status and perspectives, Atmos. Chem. Phys., 18(7), 4935-4964, 2018

Morgan, W. T., Allan, J. D., Bauguitte, S., Darbyshire, E., Flynn, M. J., Lee, J and Coe, H: Transformation and aging of biomass burning carbonaceous aerosol over tropical South America from aircraft in-situ measurements during SAMBBA, 2019

Müller, D., Ansmann, A., Mattis, I., Tesche, M., Wandinger, U., Althausen, D., and Pisani, G.: Aerosol-type-dependent lidar ratios observed with Raman lidar, J. Geophys. Res., 112, D16202, https://doi.org/10.1029/2006JD008292, 2007

Nakajima, T., Tonna, G., Rao, R., Kaufman, Y., and Holben, B.: Use of sky brightness measurements from ground for remote sensing of particulate polydispersions. Appl. Optics, 35, 2672–2686, 1996

Neumann, C.: Global guide to tropical cyclone forecasting, WMO Trop. Cyclone Program Rep. TCP-31, chap. Global Overview, World Meteorol. Organ., Geneva, Switzerland, 43 pp., 1993

Nicolae, D., Nemuc, A., Müller, D., Talianu, C., Vasilescu, J., Belegante, L. and Kolgotin, A. : Characterization of fresh and aged BB events using multiwavelength Raman lidar and mass spectrometry. Journal of Geophysical Research: Atmospheres, 118(7), 2956-2965, 2013

Ohneiser, K., Ansmann, A., Kaifler, B., Chudnovsky, A., Barja, B., Knopf, D. A and Zamorano, F.: Australian wildfire smoke in the stratosphere: the decay phase in 2020/2021 and impact on ozone depletion. Atmospheric Chemistry and Physics, 22(11), 7417, 2022

Ohneiser, K., Ansmann, A., Baars, H., Seifert, P., Barja, B., Jimenez, C and Wandinger, U.: Smoke of extreme Australian bushfires observed in the stratosphere over Punta Arenas, Chile, in January 2020: optical thickness, lidar ratios, and depolarization ratios at 355 and 532 nm. Atmospheric Chemistry and Physics, 20(13), 8003-8015, 2020

Pisso, I., Sollum, E., Grythe, H., Kristiansen, N. I., Cassiani, M., Eckhardt, S., Arnold, D., Morton, D., Thompson, R. L., Groot Zwaaftink, C. D., Evangeliou, N., Sodemann, H., Haimberger, L., Henne, S., Brunner, D., Burkhart, J. F., Fouilloux, A., Brioude, J., Philipp, A., Seibert, P., and Stohl, A.: The Lagrangian particle dispersion model FLEXPART version 10.4, Geosci. Model Dev., 12, 4955–4997, https://doi.org/10.5194/gmd-12-4955-2019, 2019.

Portafaix, T., Morel, B., Bencherif, H., Baldy, S., Godin-Beekmann, S., and Hauchecorne, A.: Fine-scale study of a thick stratospheric ozone lamina at the edge of the southern subtropical barrier, J. Geophys. Res.-Atmos., 108, D64196, https://doi.org/10.1029/2002JD002741, 2003.

Pumphrey, H. C., Filipiak, M. J., Livesey, J., Scwartz, M. J., Boone, C., Walker, K. A., Bernath, P., Ricaud, P., Barret, B., Clerbaux, C., Jarnot, R. F., Manney, G. L. and Waters, J. W:

Validation of middle-atmosphere carbon monoxide retrievals from the Microwave Limb Sounder on Aura, J. Geophys. Res., 112, D24S38, doi: 10.1029/2007JD008723, 2007.

Russell-Smith, J.; Yates, C.P.; Whitehead, P.J.; Smith, R.; Craig, R.; Allan, G.E.; Thackway, R.; Frakes, I.; Cridland, S.;Meyer, M.C.P.; et al. Bushfires' down under': Patterns and implications of contemporary Australian landscape burning. Int. J.Wildland Fire, 16, 361–377, 2007

Sakai, T., T. Nagai, M. Nakazato, Y. Mano, and T. Matsumura: Ice clouds and Asian dust studied with lidar measurements of particle extinction-to-backscatter ratio, particle depolarization, and water vapor mixing ration over Tsukuba. Applied Optics 42 7103 –7116, 2003

Sakai, T., O. Uchino, T. Nagai, B. Liley, I. Morino, and T. Fujimoto: Long-term variation of stratospheric aerosols observed with lidars over Tsukuba, Japan, from 1982 and Lauder, New Zealand, from 1992 to 2015, J. Geophys. Res. Atmos., 121, 10,283–10,293, doi:10.1002/2016JD025132, 2016

Santee, M. L., Lambert, A., Manney, G. L., Livesey, N. J., Froidevaux, L., Neu, J. L. and Ward, B. M: Prolonged and pervasive perturbations in the composition of the Southern Hemisphere midlatitude lower stratosphere from the Australian New Year's fires. Geophysical Research Letters, 49(4), e2021GL096270, 2022

Schwartz, M. J., Santee, M. L., Pumphrey, H. C., Manney, G. L., Lambert, A., Livesey, N. J., and Werner, F: Australian new year's pyrocb impact on stratospheric composition. Geophysical Research Letters, 47(24), e2020GL090831, 2020

Schoeberl, M. R., Douglass, A. R., Hilsenrath, E., Bhartia, P. K.,Barnett, J., Beer, R., Waters, J., Gunson, M., Froidevaux, L.,Gille, J., Levelt, P. F., and DeCola, P.: Overview of the EOS Aura Mission, IEEE Trans. Geosci. Remote Sens., 44, 1066–1074, 2006.

Sellitto, P., Podglajen, A., Belhadji, R., Boichu, M., Carboni, E., Cuesta, J., C. Duchamp, C. Kloss, R. Siddans, N. Bègue, L. Blarel, F. Jegou, S. Khaykin, J. -B. Renard. and Legras, B.: The unexpected radiative impact of the Hunga Tonga eruption of 15th January 2022. Communications Earth & Environment, 3(1), 1-10., 2022

Sofiev, M., Ermakova, T. and Vankevich, R.: Evaluation of the smoke-injection height from wild-land fires using remote-sensing data. Atmospheric Chemistry and Physics, 12(4), 1995-2006, 2012

Solomon, S., Stone, K., Yu, P., Murphy, D. M., Kinnison, D., Ravishankara, A. R and Wang, P: Chlorine activation and enhanced ozone depletion induced by wildfire aerosol, Nature, 615(7951), 259-264, 2023

Swap, R. J., Annegarn, H. J., Suttles, J. T., King, M. D., Platnick, S., Privette, J. L and Scholes, R. J: Africa burning: a thematic analysis of the Southern African Regional Science Initiative (SAFARI 2000). Journal of Geophysical Research: Atmospheres, 108(D13), 2003

Taha, G., Loughman, R., Zhu, T., Thomason, L., Kar, J., Rieger, L. and Bourassa, A: OMPS LP Version 2.0 multi-wavelength aerosol extinction coefficient retrieval algorithm., Atmospheric Measurement Techniques, 14(2), 1015-1036, 2021

Tencé, F., Jumelet, J., Bekki, S., Khaykin, S., Sarkissian, A. and Keckhut, P.: Australian Black Summer smoke observed by lidar at the French Antarctic station Dumont d'Urville. Journal of Geophysical Research: Atmospheres, 127(4), e2021JD035349, 2022

Turquety, S., Menut, L., Siour, G., Mailler, S., Hadji-Lazaro, J., George, M., Clerbaux, C., Hurtmans, D., Coheur, P.-F: APIFLAME v2.0 BB emissions model: Impact of refined input parameters on atmospheric concentration in Portugal in summer 2016. Geosci. Model. Dev., 2020, 13, 2981–3009, 2020.

Uchino, O., Tokunaga, M., Seki, K., Maeda, M., Naito, K., and Takahashi, K: Lidar measurement of stratospheric transmission at a wavelength of 340 nm after the eruption of El Chichon, J. Atmos. Terr. Phys., 45, 12, 849–850, 1983

Vernier, J. P., Pommereau, J. P., Garnier, A., Pelon, J., Larsen, N., Nielsen, J., and McDermid, I. S., Tropical stratospheric aerosol layer from CALIPSO lidar observations, J. Geophys. Res.-Atmos., 114, D00H10, https://doi.org/10.1029/2009JD011946, 2009

Wunch, D., Toon, G. C., Sherlock, V., Deutscher, N. M., Liu, C., Feist, D. G., and Wennberg, P. O.: The Total Carbon Column Observing Network's GGG2014 Data Version, p. 43, https://doi.org/10.14291/tccon.ggg2014.documentation.R0/122, 2015.

Young, S.A.: Analysis of lidar backscatter profiles in optically thin clouds, Appl. Opt., 34, 7019–7031., 1995

Xu, Y., Wang, W., Chen, B., Chang, M., & Wang, X.: Identification of ventilation corridors using backward trajectory simulations in Beijing. Sustainable Cities and Society, 70, 102889, 2021

Yu, P.; Davis, S.M.; Toon, O.B.; Portmann, R.W.; Bardeen, C.G.; Barnes, J.E.; Telg, H.; Maloney, C.; Rosenlof, K.H. Persistent Stratospheric Warming due to 2019–2020 Australian Wildfire Smoke. Geophys. Res. Lett. 2020, 2020, e2021GL092609, 2020

Yu, P., Davis, S. M., Toon, O. B., Portmann, R. W., Bardeen, C. G., Barnes, J. E and Rosenlof, K. H: Persistent stratospheric warming due to 2019–2020 Australian wildfire smoke. Geophysical Research Letters, 48(7), e2021GL092609, 2021

Zhou, M., Langerock, B., Vigouroux, C., Sha, M. K., Ramonet, M., Delmotte, M., ... & De Mazière, M.: Atmospheric CO and CH 4 time series and seasonal variations on Reunion Island from ground-based in situ and FTIR (NDACC and TCCON) measurements. Atmospheric Chemistry and Physics, 18(19), 13881-13901, 2018

FIGURES AND TABLE

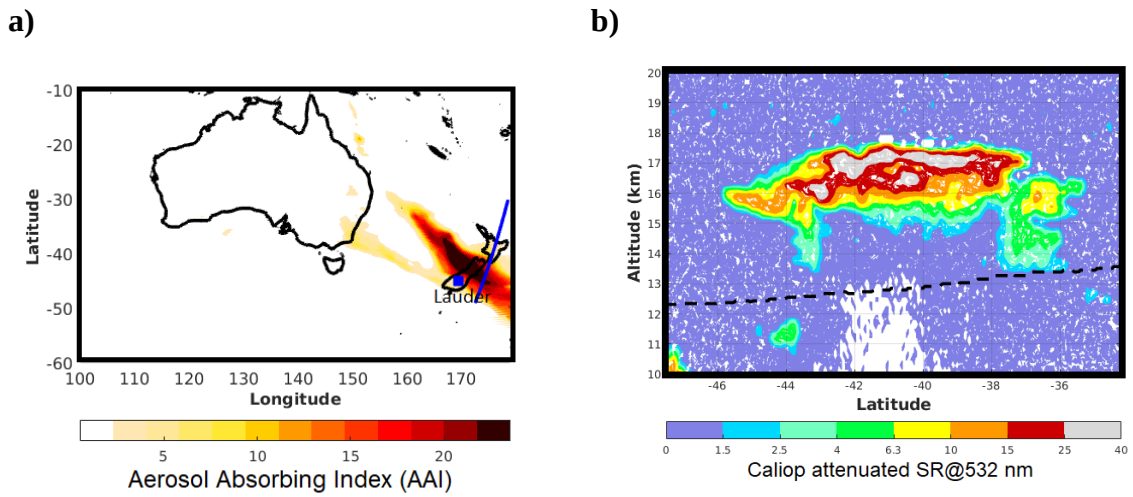

Figure 1: (a) Map of Aerosol Absorbing Index obtained from OMPS observations and **(b)** scattering ratio profiles at 532 nm obtained from CALIOP observations on 1st January 2020. The orbit overpass of CALIOP is indicated by the blue curve, while the blue square corresponds to the Lauder site in plot (a). The black dashed line in (b) corresponds to the 380 K isentropic level calculated from CALIOP observations.

a)

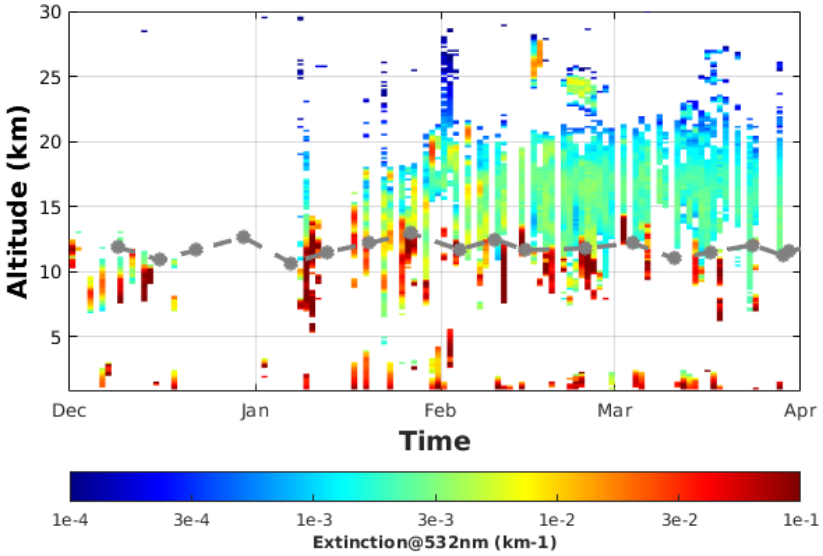

b)

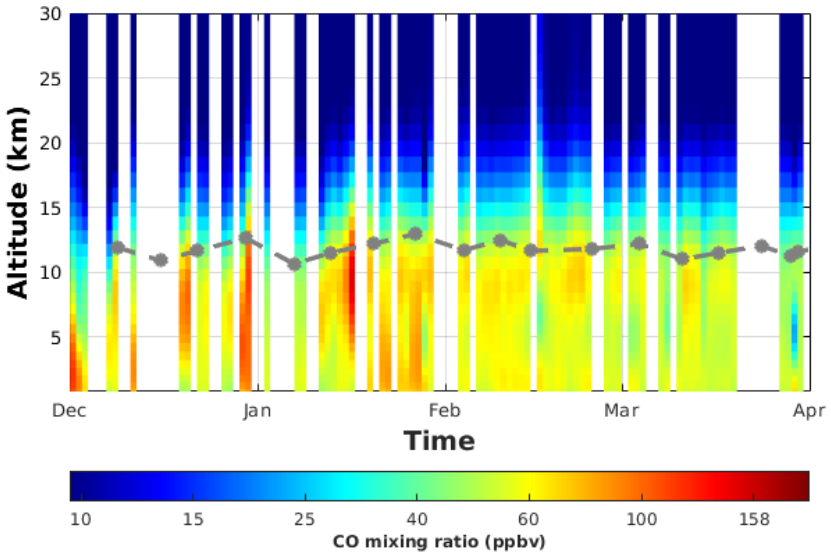

Figure 2: Time series of daily profiles at Lauder of (a) aerosol extinction at 532 nm obtained from lidar and (b) CO mixing ratio obtained from FTIR between 1st December 2019 and 1st April 2020. In order to screen non-aerosol contributors (such as clouds) **to** the extinction measurements, a mask based on the method reported by Nicolae et al. (2013)**, which** includes consideration **of** plausible aerosols properties**,** was used. **Specifically**, we only kept profile parts with positive depolarization values, and Angström exponent ranges from 0.1 to 4. The grey line indicates the tropopause height obtained from radiosonde measurements.

a)

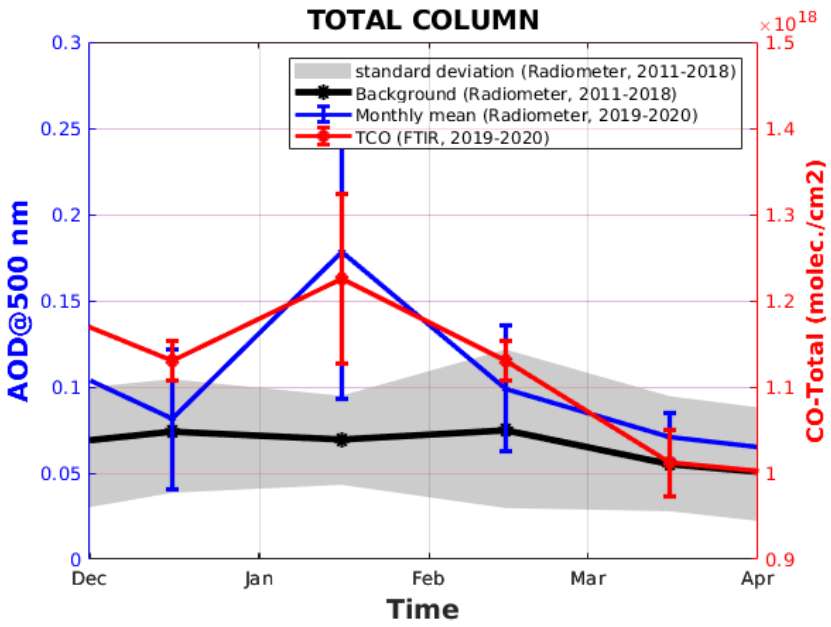

b)

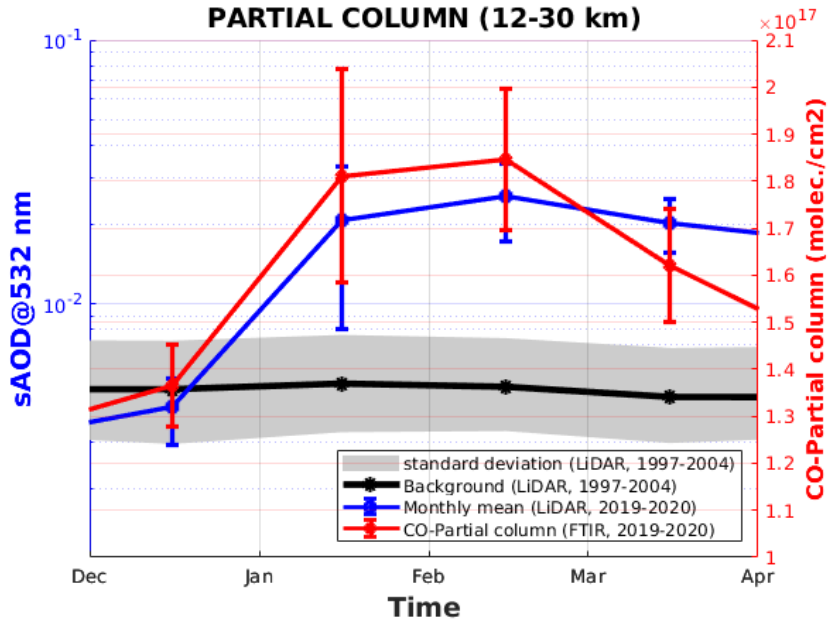

Figure 3: (a) Monthly mean evolution of total column of aerosol (AOD at 500 nm) and CO obtained from **the** SKYNET radiometer and FTIR respectively over Lauder from 1st December 2019 to 1st April 2020. **(b)** Monthly mean evolution of the stratospheric AOD (sAOD) and CO (sCO) columns at Lauder between 1st December 2019 and 1st April 2020. The sAOD and sCO are calculated between 12 and 30 km from lidar and FTIR measurements respectively. The background evolution of aerosol data (AOD: 2011-2018 and sAOD: 1997-2004) and the associated standard deviation are given in black lines and grey areas, respectively.

a)

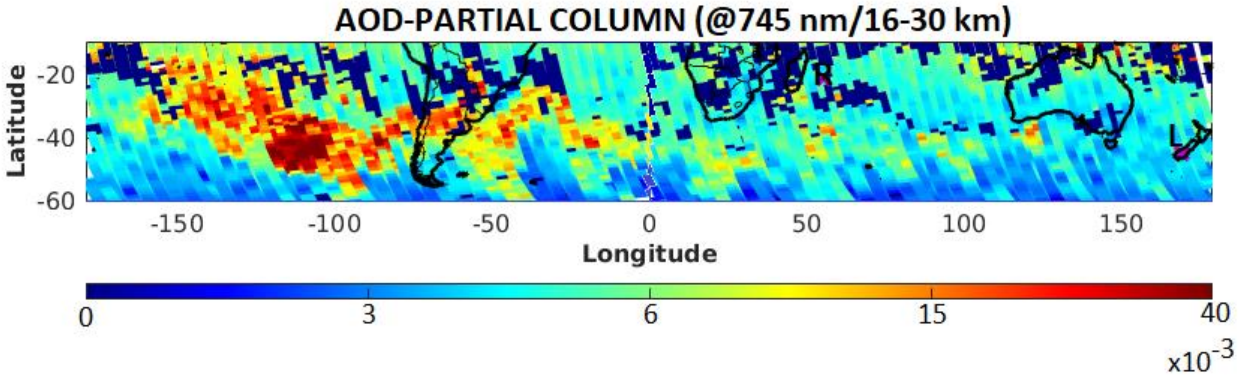

b)

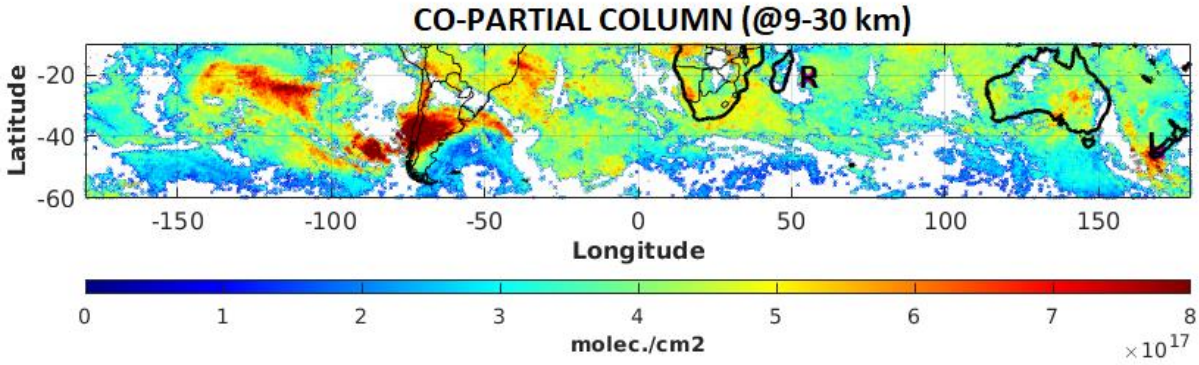

Figure 4: Time-averaged map (from 9th to 16th January 2020) of (a) sAOD (between 16 and 30 km at 745 nm) obtained from OMPS observations and (b) partial column of CO (averaged between 9 and 30 km) obtained from IASI observations. The location of Reunion and Lauder sites are indicated by R and L respectively.

1

a)

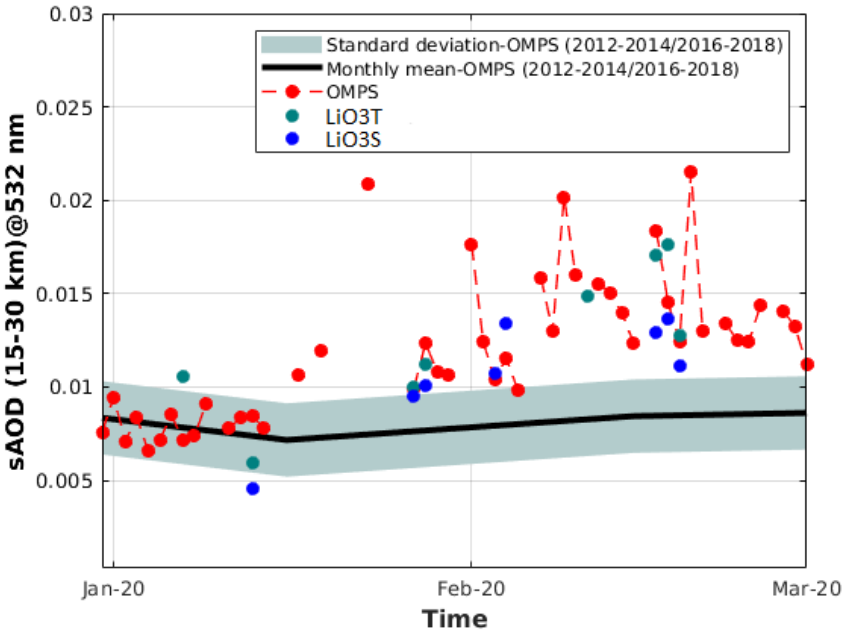

b)

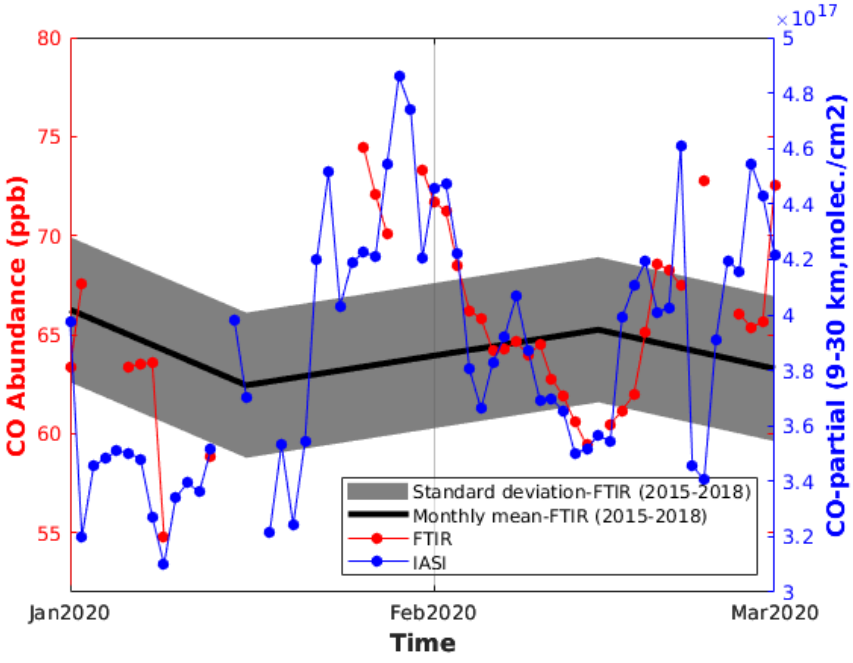

2 **Figure 5:** Daily mean evolution of aerosol (a) and CO (b) abundances obtained from ground-
3 based and satellite observations at Reunion between 1st January and 1st March 2020. Partial
4 column (molecule.cm^{-2}) and abundance (ppb) of CO obtained from IASI (blue line) and FTIR
5 (red line) respectively are given in the lower panel (b), while sAOD obtained from OMPS (red
6 line) and Lidar (blue and green dots) are given in the upper panel (a). The black and dashed
7 lines correspond to monthly mean and the associated standard deviation calculated during the
8 background period.

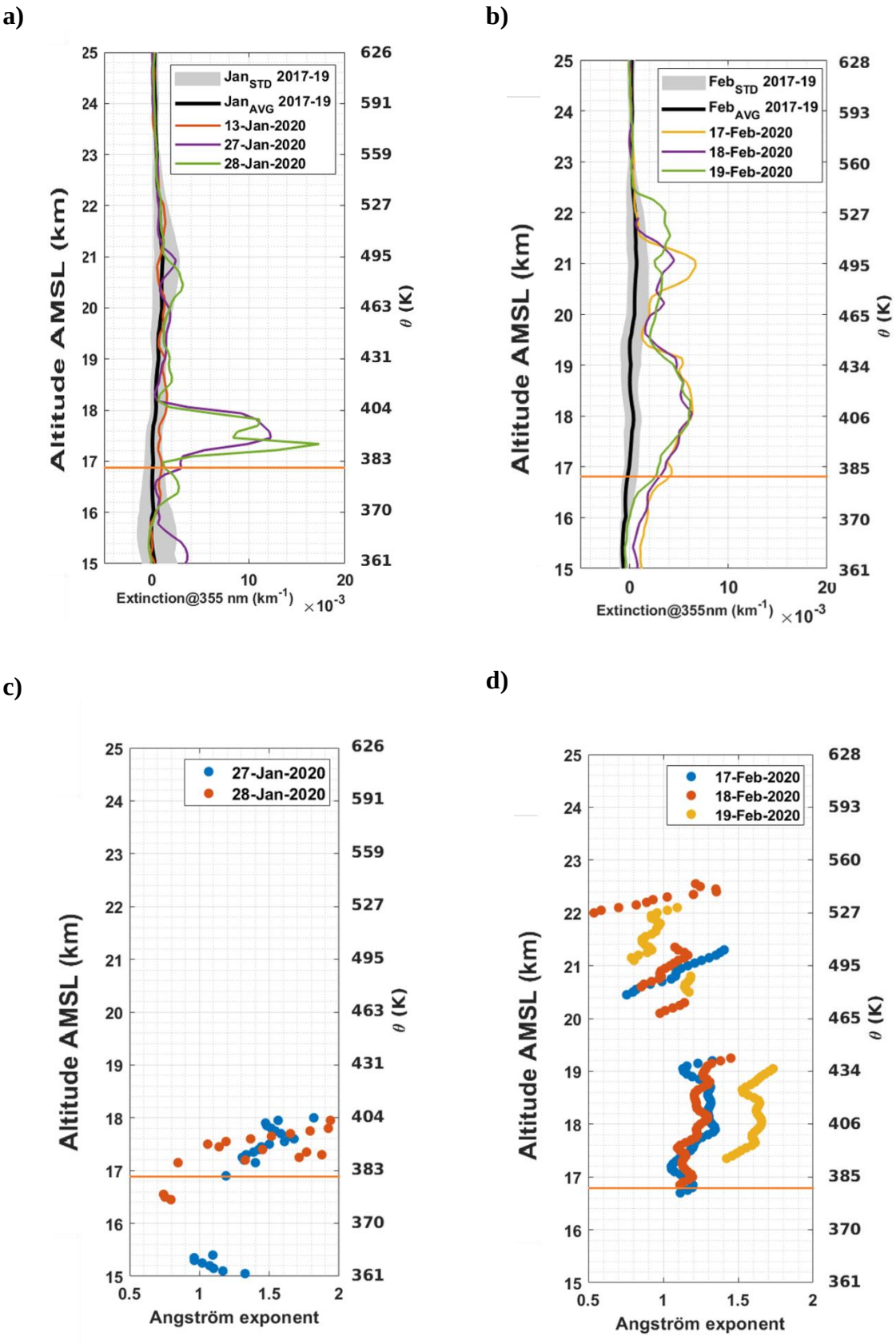

Figure 6: Aerosol extinction (at 355 nm) (a, b) and Angström exponent (355-532 nm) (c, d) obtained from lidar observations at Reunion in the months January and February 2020. The tropopause height is indicated by the orange horizontal lines.

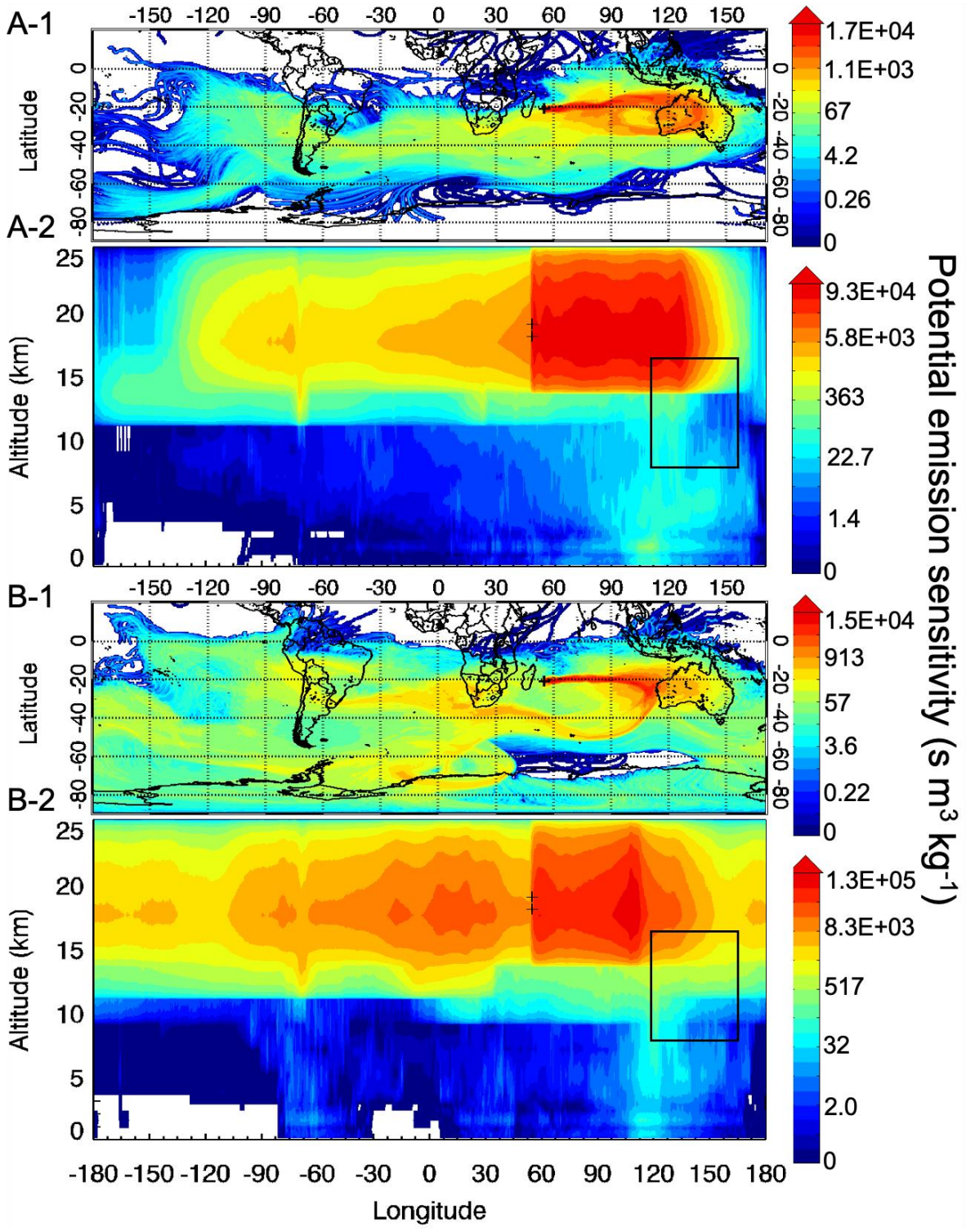

Figure 7: FLEXPART 30-day back trajectories initialized from Reunion (black cross) at 18 km on 27th January 2020 (A-1-2) and 28th January 2020 (B-1-2). A-1 and B-1 correspond to an integration of the trajectory positions over the whole altitude range. A-2 and B-2 are the vertical view integrated over the whole latitude range of the back trajectories A-1 and B-1. The black rectangle represented the injection height of the biomass burning aerosols.

a)

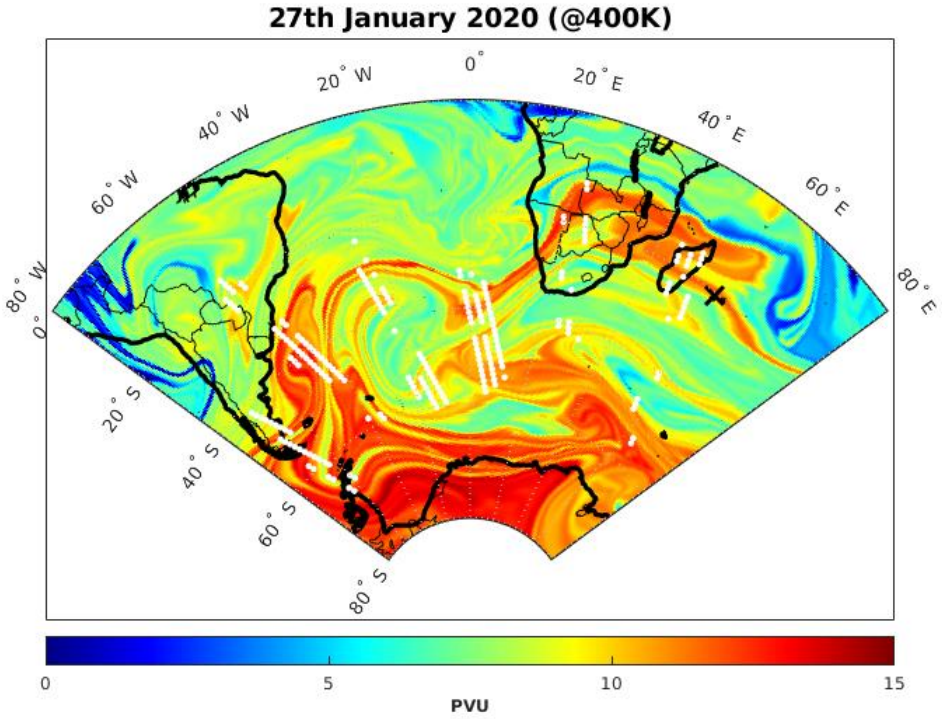

b)

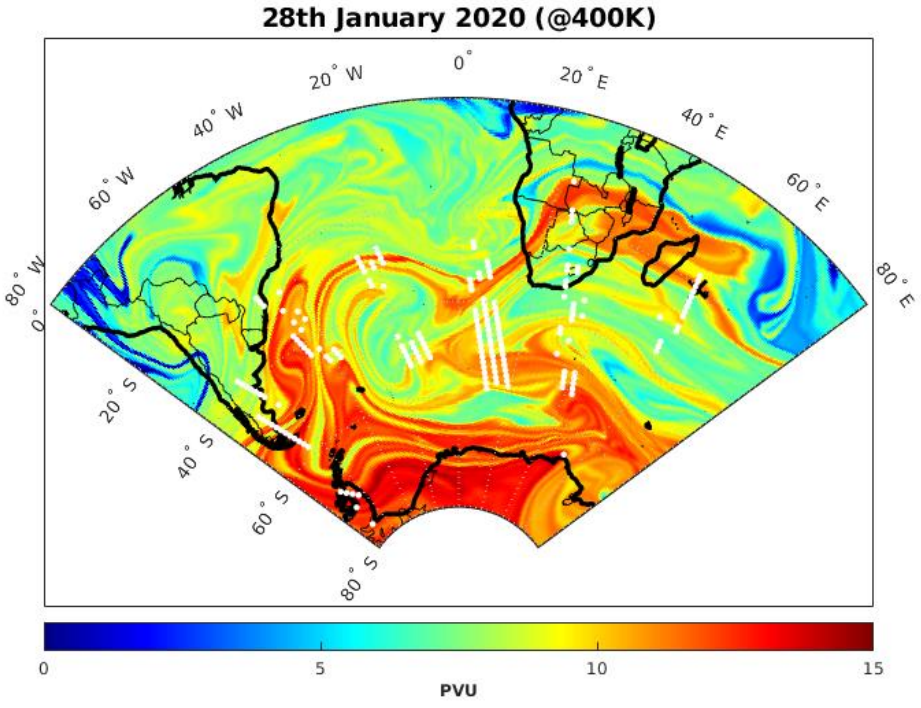

Figure 8: Advected PV map at the 400 K level obtained from the MIMOSA model (a) on 27 January 2022 and (b) on 28 January 2022. The white dots represent the localization of the aerosol plume at 400 K ± 5 K obtained from OMPS observations, while the black cross indicates Reunion.

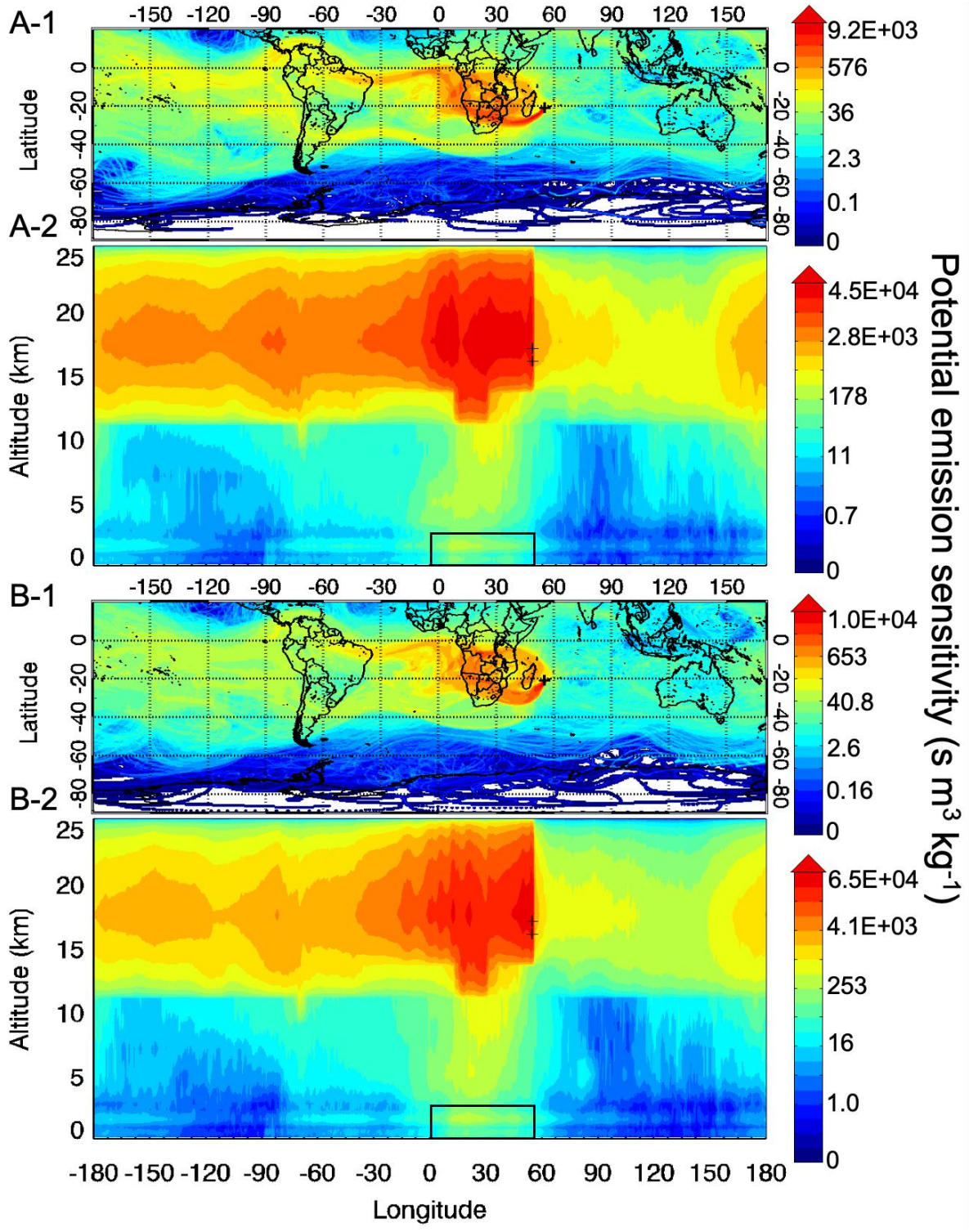

Figure 9: Same as figure 7 with an injection height initialized at 16 km.

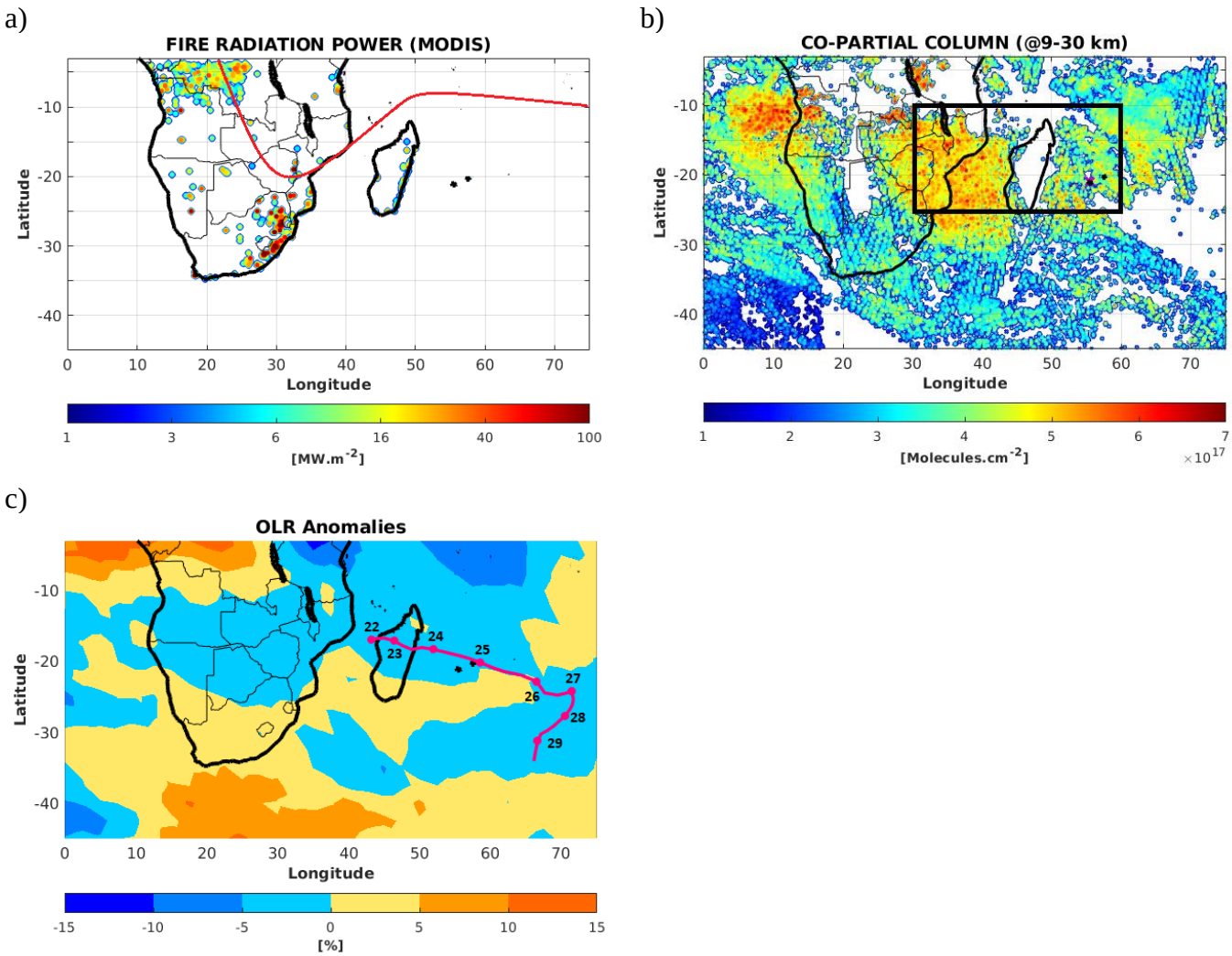

Figure 10: a) The total number of fire pixel and the associated fire radiative power obtained from MODIS observation between 16th and 29th January 2020. The red line indicates the average position of ITCZ (from Lashkari et al., 2017). b) Time-average map of partial column of CO (calculated between 9 and 30 km) obtained from IASI observations averaged between 16th and 29th January 2020. The black square corresponds to the study domain where the vertical cross-section of CO and water vapor mixing ratio are calculated and reported in Figure 11. c) Time-average map of outgoing longwave radiation anomalies obtained from NCEP between 16th and 29th January 2020. The red curve corresponds the trajectory followed by the Diane strong tropical storm from 22nd to 29th January 2020. This trajectory is obtained from the RSMC (Regional Specialized Meteorological Center) of Reunion best-track database.

a)

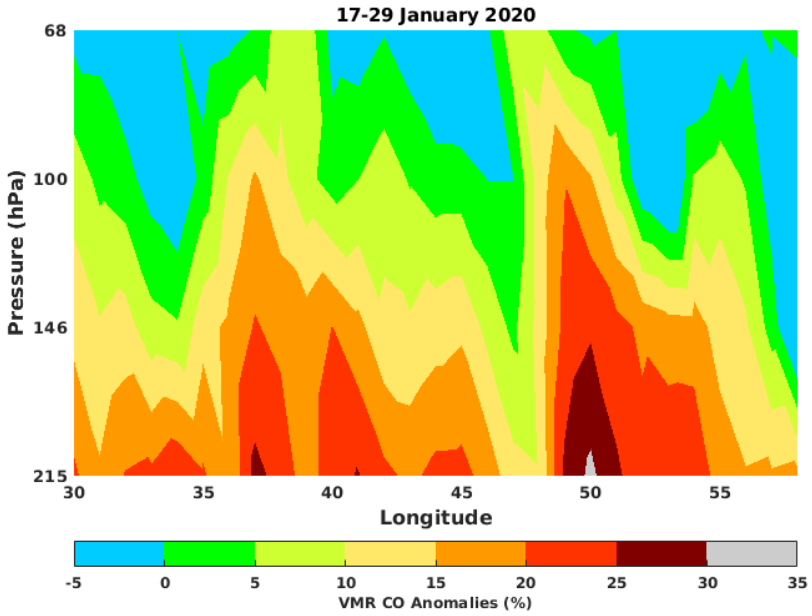

b)

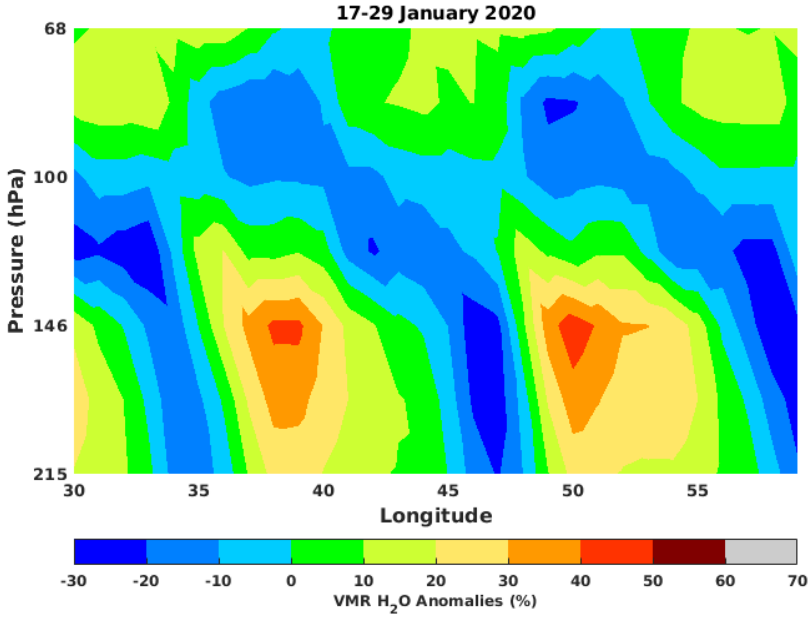

Figure 11: Vertical cross section of (a) CO and (b) water vapor mixing ratio anomalies obtained from MLS observation over southern Africa and the SWIO basin (black box in Figure 10b) between 16th and 29th January 2020.

a)

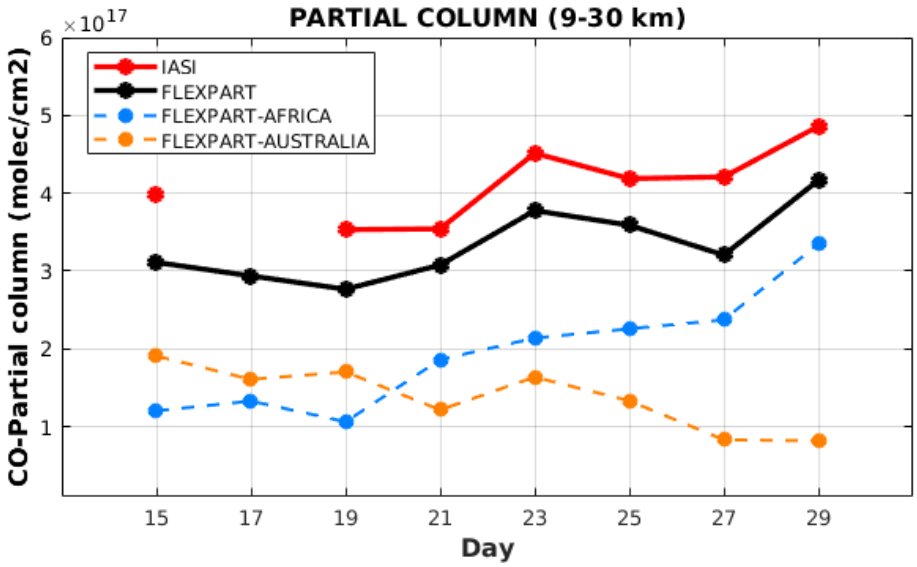

b)

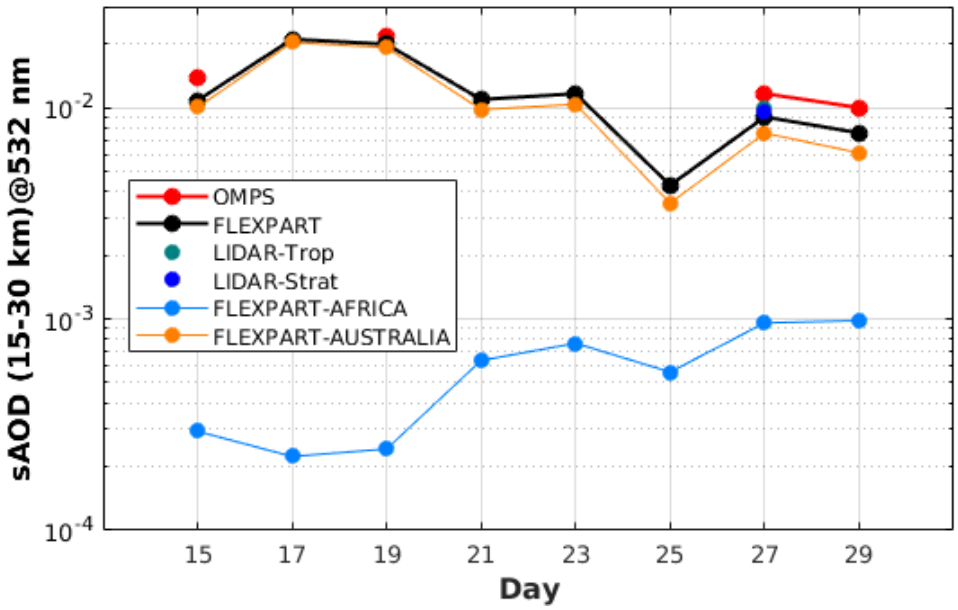

Figure 12: a) Daily evolution of partial column (calculated between 9 and 30 km) of CO observed by IASI (red line) and simulated by FLEXPART (black line) over Reunion from 15th to 29th January 2020. The CO evolution is simulated by FLEXPART considering only the CO emission (including BB and anthropogenic activity). b) Daily evolution of sAOD (calculated between 15 and 30 km at 532 nm) obtained from **OMPS-LP** (red line), lidar (blue dots) and simulated by FLEXPART (black line) over Reunion from 15th to 29th January 2020. The simulated sAOD are calculated in considering only the aerosol emission (BC and OC).). The contribution from the African and Australian emission are in cyan line and orange line, respectively.